



UNIVERSITY OF LEEDS

This is a repository copy of *Effect of a Pore Throat Microstructure on Miscible CO₂ Soaking Alternating Gas Flooding of Tight Sandstone Reservoirs*.

White Rose Research Online URL for this paper:
<https://eprints.whiterose.ac.uk/162966/>

Version: Accepted Version

Article:

Wang, Q, Wang, L, Glover, PWJ orcid.org/0000-0003-1715-5474 et al. (1 more author)
(2020) Effect of a Pore Throat Microstructure on Miscible CO₂ Soaking Alternating Gas Flooding of Tight Sandstone Reservoirs. *Energy & Fuels*. ISSN 0887-0624

<https://doi.org/10.1021/acs.energyfuels.0c01431>

© 2020 American Chemical Society. This is an author produced version of a journal article published in *Energy & Fuels*. Uploaded in accordance with the publisher's self-archiving policy.

Reuse

Items deposited in White Rose Research Online are protected by copyright, with all rights reserved unless indicated otherwise. They may be downloaded and/or printed for private study, or other acts as permitted by national copyright laws. The publisher or other rights holders may allow further reproduction and re-use of the full text version. This is indicated by the licence information on the White Rose Research Online record for the item.

Takedown

If you consider content in White Rose Research Online to be in breach of UK law, please notify us by emailing eprints@whiterose.ac.uk including the URL of the record and the reason for the withdrawal request.



eprints@whiterose.ac.uk
<https://eprints.whiterose.ac.uk/>

Effect of pore-throat microstructure on miscible CO₂ soaking-alternating-gas (CO₂-SAG) flooding of tight sandstone reservoirs

Qian Wang^{1,3}, Lu Wang^{1*}, Paul W.J. Glover², Piroska Lorinczi²

1 State Key Laboratory of Oil and Gas Reservoir Geology and Exploitation, Chengdu University of Technology, Chengdu, Sichuan, 610059, China

2 School of Earth and Environment, University of Leeds, Leeds, LS2 9JT, UK

3 School of Petroleum Engineering, China University of Petroleum-Beijing, Beijing 102249, China

*Correspondence: wlhmhxydh@163.com

Abstract: Miscible CO₂-SAG flooding is an improved version of CO₂ flooding, which compensates for the insufficient interaction of CO₂ and crude oil in the reservoir by adding a CO₂ soaking process after the CO₂ breakthrough (BT). The transmission of CO₂ in the reservoir during the soaking process is controlled by the pore-throat structure of the formation, which in turn affects the displacement efficiency of the subsequent secondary CO₂ flooding. In this work, CO₂-SAG flooding experiments at reservoir conditions (up to 70°C, 18 MPa) have been carried out on four samples with very similar permeabilities, but significantly different pore size distributions and pore-throat structures. The results have been compared with the results of CO₂ flooding on the same samples. It was found that the oil recovery factors (RFs) when using CO₂-SAG flooding are higher than when using CO₂ flooding by 8-14%. In addition, we find greater improvements in RF for rocks with greater heterogeneity of their pore-throat microstructure compared with CO₂ flooding. The CO₂ soaking process compensates effectively for the insufficient interaction between CO₂ and crude oil due to premature CO₂ BT in heterogeneous cores. Moreover, rocks with a more homogeneous pore-throat microstructure exhibit a higher pressure decay rate in the CO₂ soaking process. The initial rapid pressure decay stage lasts 80-135 minutes (in our experimental cores), accounting for over 80% of the total decay pressure. Rocks with the larger and more homogeneous pore-throat microstructure exhibit smaller permeability decreases due to asphaltene precipitation after CO₂-SAG flooding, possibly because the permeability of rocks with more heterogeneous and smaller pore-throat microstructure is more susceptible to damage from asphaltene precipitation. However, the overall permeability decline is 0.6-3.6% higher than that of normal CO₂ flooding due to the increased time for asphaltene precipitation. Nevertheless, the corresponding permeability average decline per 1% oil RF is 0.11-0.34%, which is lower than that for CO₂ flooding, making the process worthwhile. We have shown that CO₂-SAG flooding has the potential to improve oil RFs with relatively little damage to cores, especially for cores with small and heterogeneous pore-throat microstructures, but for which severe wettability changes due to the CO₂ soaking process can become significant.

Keywords: CO₂ and CO₂-SAG flooding, pore-throat structure, oil RFs, pressure decay, permeability decline, asphaltene precipitation

Introduction

Tight sandstone reservoirs are characterized by poor reservoir quality and complex pore-throat microstructures, which makes them difficult to develop and often results in low RFs^[1-3]. Accurate evaluation of the reservoir pore-throat microstructure is a prerequisite for effective field development. Fractal theory is an effective method for investigating physical properties of rocks^[4-5]. This approach builds a bridge between micro-morphology (pore size and shape, pore size distribution, pore connectivity) and macro performance (porosity, permeability) to characterize complexity and irregularity of pore-throats structure^[6-8]. The process of CO₂ flooding has proven to be an effective enhanced oil recovery (EOR) method in tight sandstone reservoirs^[9-10]. The main mechanisms of CO₂-EOR techniques include (i) the oil-swelling effect, (ii) viscosity reduction, (iii) light-hydrocarbon extraction, and (iv) the reduction of interfacial tension (IFT). They can achieve higher efficiency if carried out at miscible conditions^[11-12]. However, CO₂-EOR techniques suffer from asphaltene precipitation, which can lead to significant reductions in formation permeability and water wettability. Asphaltenes begin to precipitate from the crude oil and aggregate when CO₂ is injected into cores and reaches a critical value. Some asphaltene particles remain mobile, and migrate with the pore fluid, causing blockages of the pores and pore-throats, while other asphaltene particles are adsorbed onto pore surfaces, resulting in permeability decline and making the rock more oil wet^[13-17].

There are a number of different types of CO₂-EOR techniques, the predominant ones include (i) continuous miscible CO₂ injection, (ii) carbonated water injection (CWI), (iii) water-alternating-gas (WAG) injection, and (iv) the so-called CO₂ huff-and-puff technique. The CO₂-WAG injection process controls the mobility ratio of the displacing phase to the displaced phase by injecting water and CO₂ slugs alternately, resulting in a high displacement efficiency of the injected CO₂ and a relatively high sweep efficiency of the injected water^[18]. Nevertheless, there is still a lot of residual oil trapped in reservoirs, and it becomes more difficult to access and recover the oil due to water-blocking after CO₂-WAG flooding^[19]. The CWI technique combines the advantages of water-flooding and CO₂ flooding together by dissolving CO₂ into water prior to injection. However, the actual performance of CWI is considerably compromised because of the low solubility of CO₂ in water, and also the low injectability of water in a tight oil formation, similar to CO₂-WAG^[20]. The major EOR mechanism of CO₂ huff-and-puff relies on solvent molecular diffusion rather than solvent convective dispersion. The ultimate contact or drainage area of the injected CO₂ is relatively

small. Continuous miscible CO₂ injection has high oil displacement efficiency, simple injection operation and low cost. However, it produces an untimely CO₂ BT caused by viscous fingering, gravity segregation mechanisms and reservoir heterogeneity^[21-22].

The CO₂-SAG flooding process, as a modified EOR method, combines the continuous miscible CO₂ flooding and the CO₂-soaking process from the CO₂ huff-and-puff processes^[23]. More specifically, at first, CO₂ is injected continuously into the reservoirs to displace oil until the CO₂ BT. In the subsequent CO₂-soaking period, both the injector and producer are shut in so that the injected CO₂ diffuses into those residual reservoir fluids that were not previously in contact with CO₂ due to the early CO₂ BT. As the CO₂ concentration in the residual oil increases, the oil viscosity decreases dramatically, the oil swells and enters the previous CO₂ flow paths or CO₂ BT channels^[24]. Moreover, CO₂ also effectively extracts the light components of crude oil during the CO₂-soaking period. The combination of these effects allows the subsequent secondary CO₂ flooding to displace and recover more residual oil^[25].

By comparison with the other CO₂-EOR processes, the solvent convective dispersion in the CO₂-SAG process results in a much higher CO₂ dissolution efficiency in crude oil than that in the solvent molecular diffusion in the CO₂ huff-and-puff process. Moreover, CO₂ has a much longer retention time to fully interact with the residual oil and reservoir brine during the CO₂-soaking period, which substantially increases CO₂ sweep and displacement efficiency in the secondary CO₂ flooding, with higher CO₂ utilization efficiency and lower injection cost than continuous CO₂ flooding^[24].

Unfortunately there have been only a few core-flooding experiments conducted to study the technical advantages and actual potential of CO₂-SAG injection, including the effects of CO₂ injection pressures, injection flow rate, CO₂ soaking time and pre-waterflooding^[24-25]. Furthermore, compared with miscible CO₂ flooding, the effects of asphaltene precipitation, reservoir permeability damage, and the relationship between pressure decay and soaking time during CO₂ soaking in CO₂-SAG flooding remains, to our knowledge, if not unstudied, then unpublished. In addition, the effect of the heterogeneity of the pore-throat structure on the efficiency of CO₂-SAG flooding has not been studied at all.

This paper examines the efficacy of the CO₂-SAG flooding process with particular focus on oil recovery factors, peri-soaking pressure declines, asphaltene precipitation and transport, and permeability damage, providing data and analysis that is currently not available in the scientific

literature. The effects of all of these factors have been considered with regard to the relative heterogeneity of the pore microstructure. All of the results have been compared to the results of a similar study on the process of continuous miscible CO₂ flooding (Wang et al., 2020)^[13] in order to understand the advantages and disadvantages of each. This comparison was possible because both sets of results were made on the same 4 cores, each of which shared the similar permeability but exhibited a different pore-throat structure and different degrees of heterogeneity of the pore-throat microstructure.

Methodology

Materials

The oil sample was collected from a typical low-permeability sandstone reservoir with a depth of 2100-2400 m in the large Changqing Oilfield, which is located near Yulin in the Shaanxi province of China. The crude oil used in the experiments is synthetic live oil (Table 1), which was prepared in the laboratory based on the produced oil composition (Table 1). The content of *n*-C₅ insoluble asphaltene in the crude oil was measured to be 1.32 wt% by using the standard ASTM D2007-03 method. The minimum miscible pressure (MMP) of the crude oil-CO₂ system at 70±0.1°C is 16.8±0.3 MPa measured by slim-tube apparatus and published in previous work. Two types of brine (ordinary brine and Mn²⁺-doped brine) were used in our experiments. Each was prepared according to the composition of formation water, which consists predominantly of dissolved calcium chloride with a total dissolved solids (TDS) of 29520 mg/dm³ (Table 2). The Mn²⁺-doped brine was prepared in the same way as the ordinary brine, but with the addition of 15,000 mg/dm³ of MnCl₂. The addition of Mn²⁺ ions is to shield the water signal during nuclear magnetic resonance (NMR) tests in order to obtain the oil distribution in the core^[14]. The detailed basic physical properties of the synthetic live oil and formation water are reported in previously published papers^[12-13].

Four core samples with similar permeability values but clearly distinct NMR transversal relaxation time (T₂) distributions were selected from 237 core samples from the same sandstone reservoir (Table 3 and Figure 1). The NMR spectrometer (Mini-MR, Niumag, Suzhou, China) has a frequency range of 1-30 MHz, and was operated with a magnetic intensity of 0.5T). This apparatus can detect the transverse relaxation motion of hydrogen nuclei of fluids in the pores, and represents it as a T₂ spectrum, which is an indicator of the distribution of fluids in pores^[26]. In our work, the T₂ range 0.1-10 ms is considered to represent small pores, and that from 10 to 1000 ms as large pores.

The pore-throat structure of these four cores was quantitatively evaluated by fractal theory based on the mercury injection capillary pressure (MICP) curve measured by constant-rate mercury injection (CRMI) tests^[13]. These tests were carried out using an APSE-730 mercury porosimeter (American Coretest Systems, Inc.) with a quasi-static constant speed of 50 nL/min and a maximum injection pressure of 6.2 MPa).

The relationship between capillary force and wetting saturation can be written as,

$$\log S = (D - 3) \log P_c + (3 - D) \log P_{min} \quad (1)$$

Where, S (fractional) is the saturation of the wetting phase corresponding to the capillary pressure, P_c is the capillary pressure (MPa), D is the fractal dimension (unitless), P_{min} is the capillary pressure corresponding to the largest pore-throat (MPa).

A linear relationship exists between the logarithm of the capillary pressure and the corresponding logarithm of the saturation of the wetting phase (mercury is the non-wetting phase). Consequently, the CRMI test results for linear regression analysis can be used to obtain the pore fractal dimension D for drainage. The fractal dimension in the three-dimensional Euclidean space is between 2 and 3. The value of fractal dimension is a representation of rock heterogeneity^[5,7-8], increasing continuously as the complexity of pore network increases. In other words, the greater the fractal dimension, the greater the heterogeneity of pore structure^[27]. The fractal dimensions of small pore-throat structure calculated from the CRMI tests can be ranked in increasing order: H3 (2.596) < H2 (2.622) < H1 (2.706) < H4 (2.748), indicating that the pore-throat structures of H2 and H3 are less heterogeneous than those of H1 and H4. In addition, there is no significant difference in the pore distribution of the four cores (**Figure 1**). Pore-throats play a dominant role in controlling the permeability of cores^[28]. The pore-throat distributions of H1 and H4 are wider than those of H2 and H3, implying that H2 and H3 have narrower pore-throat distributions. Moreover, the distributions of pore-throat ratio also imply that H1 and H4 have strong heterogeneity in pore-throat microstructure.

Table 1. Basic physical properties of live oil together with its compositional analysis (*n*-C5 insoluble asphaltene content =1.32 wt%).

Property		Value			
Density (g/cm ³)		0.725±0.002 (70°C)			
Viscosity (cP)		3.88±0.05 (70°C)			
Solution gas-oil ratio (m ³ /m ³)		31.4			
Bubble point pressure (MPa)		7.52			
Composition					
Carbon number	wt%	Carbon number	wt%	Carbon number	wt%
CO ₂	0.08	C ₉	6.46	C ₂₁	1.80
N ₂	0.31	C ₁₀	5.70	C ₂₂	1.92
C ₁	1.50	C ₁₁	4.86	C ₂₃	1.67
C ₂	0.60	C ₁₂	4.21	C ₂₄	1.74
C ₃	0.49	C ₁₃	4.28	C ₂₅	1.59
<i>i</i> C ₄	0.25	C ₁₄	4.45	C ₂₆	1.56
<i>n</i> C ₄	0.47	C ₁₅	3.88	C ₂₇	1.58
<i>i</i> C ₅	1.18	C ₁₆	3.38	C ₂₈	1.48
<i>n</i> C ₅	0.22	C ₁₇	3.08	C ₂₉	1.40
C ₆	4.86	C ₁₈	2.93	C ₃₀₊	15.78
C ₇	5.55	C ₁₉	2.38	Total	100
C ₈	6.10	C ₂₀	2.28		

Table 2. Physicochemical properties of the reservoir brine.

Item	Value
Density (g/cm ³)	1.01
Viscosity at 25°C (cP)	1.03
pH	7.04
K ⁺ (mg/L)	296
Na ⁺ (mg/L)	3494
Ca ²⁺ (mg/L)	7134
Mg ²⁺ (mg/L)	48.2
Cl ⁻ (mg/L)	18433
SO ₄ ²⁻ (mg/L)	114
TDS (mg/L)	29520

Table 3. Basic parameters of the core samples.

Core number	Length (cm)	Diameter (cm)	Permeability (mD)	Porosity (%)
H1	5.11	2.54	0.713	14.62
H2	5.07	2.54	0.742	14.14
H3	5.09	2.53	0.769	13.62
H4	5.02	2.54	0.734	11.85

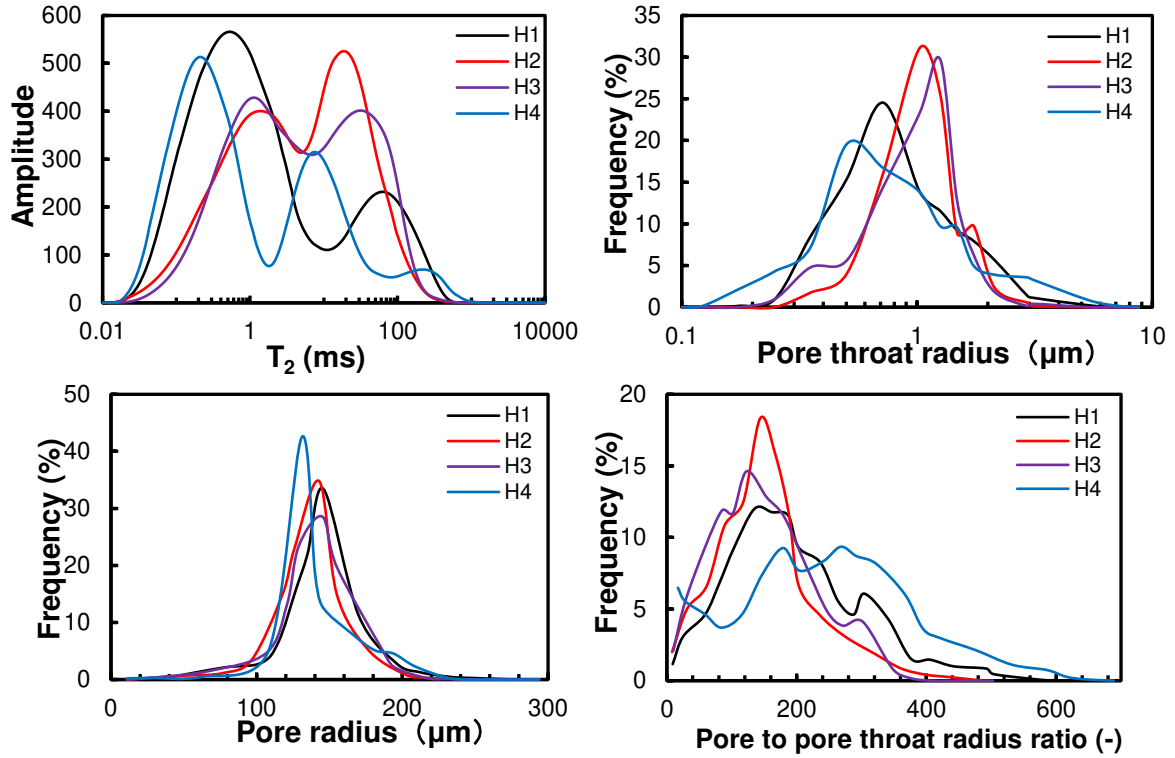


Figure 1. NMR and MICP results before experiments. The upper left panel shows the T₂ spectrum of four cores in fully saturated brine before experiments obtained by NMR tests, reflecting the pore size distribution of the four cores. The other three graphs are the distributions of throat radius, pore radius and the pore-throat ratio before experiments according to the results of CRMI tests^[13].

Core-flooding tests

Miscible CO₂ flooding experiments at reservoir conditions (18 MPa, 70°C) have already been conducted on these cores. The evaluation methods and results of these flooding experiments are reported in a previously published paper and form a useful comparative dataset for the CO₂-SAG flooding carried out in this work.

Figure 2 shows the schematic diagram of the core flooding apparatus for the CO₂-SAG flooding experiments that are reported for the first time in this work. Live oil, undoped brine, brine doped with MnCl₂ (Mn²⁺, 15000 mg/dm³), and CO₂ were contained separately in four high pressure cylinders (Hongda, China; $P=80$ MPa; $T=130^{\circ}\text{C}$). A dual ISCO syringe pump was used to inject the crude oil, formation water or CO₂ from the high pressure cylinders to the core holder (Hongda, China; $P=80$ MPa; $T=130^{\circ}\text{C}$). This is a specially designed core holder for use with the NMR spectrometer. A second pump was used to maintain confining pressure, while a third pump and a back pressure valve were used in combination to regulate the back pressure. All core holders and cylinders were housed in an oven (Hongda, China; $T=150.0\pm0.1^{\circ}\text{C}$) in which the temperature was controlled to within $\pm0.1^{\circ}\text{C}$ by a three-term temperature controller.

A set of measuring devices were used to quantify the produced fluids (i.e., brine, oil, and gas). These devices included a gas-liquid separator and a mass flow meter. Pressure and flow data during the experiments were collected and logged automatically by computer.

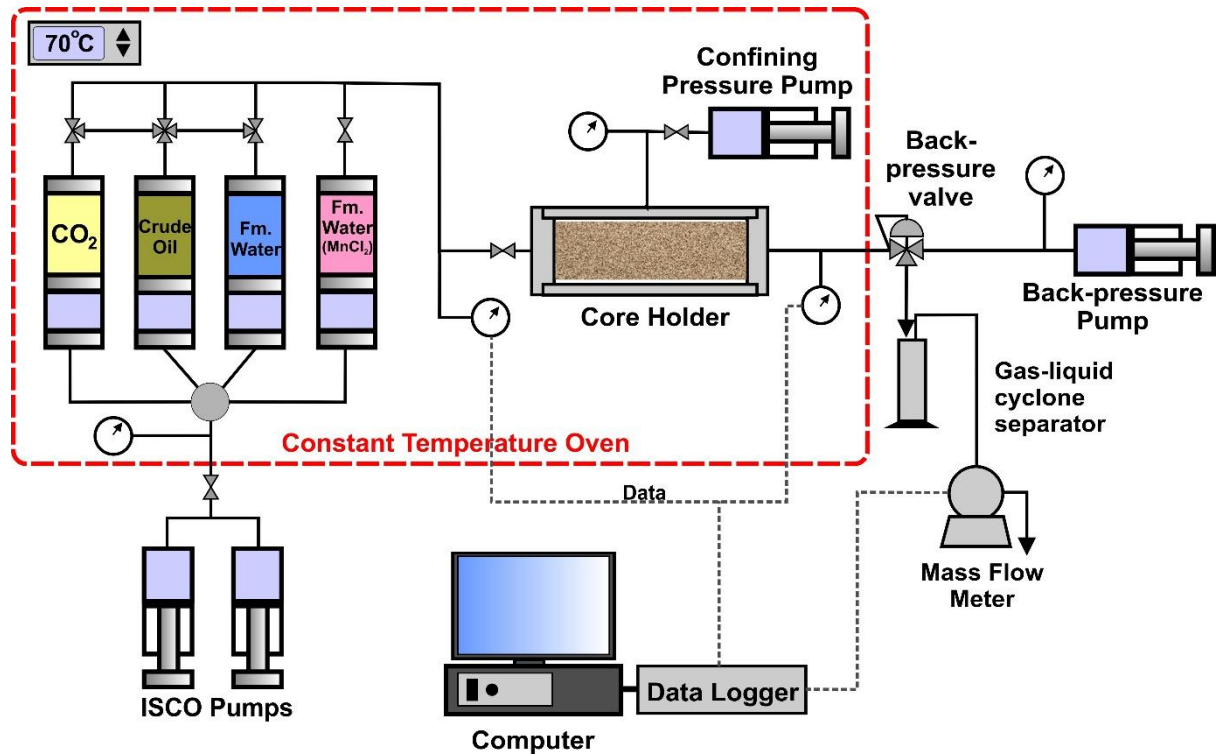


Figure 2. Schematic diagram of the miscible CO₂-WAG core-flood apparatus.

The general procedure of the core-flooding tests can be described briefly as follows.

- (1) The constant temperature oven was set to 70°C and kept at that temperature for 24 hours. The core was placed in the core holder and continuously evacuated for another 24 hours, followed by injection of brine into the core. The core was subjected to an NMR test in order to obtain the initial distribution of brine in the core. The MnCl₂ enriched brine was then injected into the core for 5 PV. The saturated core was then rescanned by the NMR apparatus to ensure that the signal of the brine had been eliminated.
- (2) Crude oil was pumped into the core to achieve the initial oil saturation (S_{oi}) and the connate water saturation (S_{wc}). The injection process was terminated after 30 hydrocarbon pore volumes (HCPV) of crude oil. The core holder was then left undisturbed for at least 24 hours in order to attain a suitable equilibrium condition at

the imposed reservoir conditions. The T_2 spectrum of the core saturated with crude oil was measured again to obtain the crude oil distribution.

- (3) In each core-flooding test, CO_2 was injected with a constant flow rate of $0.02 \text{ cm}^3/\text{min}$ into the core-holder to displace the crude oil. The pressure at the outlet of the core holder was maintained at 18 MPa.
- (4) Each core-flood was stopped when the CO_2 breakthrough (BT) occurred. The valves at the inlet and outlet of the core holder were closed during the CO_2 soaking stage. The oil distribution in the core was measured by NMR again after 5 hours when the pressures had stabilized.
- (5) Then the valves were opened and CO_2 was injected into the core holder to displace the crude oil again until no more crude oil was produced.
- (6) The injection and production pressures, and the volumes of injection and production fluid were all monitored continuously, and recorded throughout the entire flooding experiment. The core in the core holder was then re-tested by NMR to obtain the distribution of the residual oil in the core. The produced oil was collected during each core-flooding test.

Post-flooding tests

Asphaltene is soluble in aromatic solvents but not in alkanes. Consequently, all organic components except asphaltene could be cleaned from the core by extraction with *n*-heptane^[10] using a Soxhlet extractor (SXT-02, Shanghai Pingxuan Scientific Instrument CO., Ltd., China). Subsequently, the cores were dried and their porosity and gas permeability were measured. Since the extraction process left asphaltene in place, these measured porosities and gas permeabilities are those which are affected by asphaltene precipitation. The cores were immersed in brine for 24 hours for aging to eliminate the impact of saturated oil on wettability variations. The cores were saturated by ordinary brine once again and tested by NMR to obtain the T_2 spectrum of the brine distribution.

The uncertainties in the porosity measurements were assessed and calculated and found to be $<\pm 3\%$, while uncertainties in the permeability measurements were found to be about $\pm 4\%$. For each NMR assessment, NMR scanning was repeated three times to confirm the repeatability of the measurement.

Results and Discussion

This work examines CO₂-SAG flooding using the same four cores. The results of simple miscible CO₂ flooding experiments were provided in the previous paper ^[13]. Moreover, we have carried out the same core-flooding procedures during initial simple miscible CO₂ flooding up to the point of CO₂ breakthrough (BT) as in the previous paper. However, in this paper we have followed the initial flooding to BT by a soaking phase and then implemented a final CO₂ flooding. Consequently, (i) analysis of the results of this paper alone, and (ii) subsequent comparison of the results of this paper with that of the simple miscible CO₂ flooding experiments carried out earlier, makes it possible to identify those changes to oil recovery factors, permeability damage and asphaltene precipitation which result from the additional soaking phase.

Oil Recovery Factors

The T₂ spectra given in **Figure 3** show the distribution of (i) the initial oil before flooding, (ii) the residual oil at CO₂ BT, and (iii) the final residual oil (S_{or}) after the flooding was completed, for each core. The calculated oil RFs according to the NMR T₂ spectra are shown in **Table 4**.

Both this work on CO₂-SAG flooding and the previous work on simple miscible CO₂ flooding have a common procedure until CO₂ BT. It is unsurprising, therefore, that they produce very similar results when carried out on the same cores. In both cases the production rate increases during initial CO₂ flooding until it reaches a peak at CO₂ BT, which corresponds to the formation of the first channel for CO₂ transport between the inlet and outlet of the sample. For the simple miscible CO₂ flooding the ultimate oil RFs of the cores after CO₂ flooding were 4% to 7.5% higher than those at CO₂ BT. The increase in oil RF after the CO₂ BT was attributed mainly to the light hydrocarbon extraction effect of CO₂ on crude oil^[24], and it was noted that the increase in cores H2 and H3 was slightly higher than that in H1 and H4.

In this work, we have examined whether the post-BT production can be improved by instituting a period of shut-in or soaking immediately after CO₂ BT occurs, and then carrying out further miscible CO₂ core-flooding. This procedure resulted in total RF for the CO₂-SAG being 8% to 14% greater than for the miscible CO₂ core-flooding, with an increase in post-BT recovery factor increasing from 12% to 21.5%.

There is a good linear relationship ($R^2 > 0.98$) between the total RFs and the fractal dimension of the core pore-throat structure (**Figure 4**). The gradients of the relationships are negative,

indicating that higher fractal dimensions, which are associated with a greater heterogeneity in the pore microstructure provide lower recovery factors, primarily because more homogeneous rocks exhibit greater CO₂ flooding efficiency and larger CO₂ sweep volume^[12].

The slightly greater slope for the miscible CO₂ process in the RFs in **Figure 4** indicates that the miscible CO₂ process is slightly more sensitive to pore microstructure heterogeneity than the CO₂-SAG process. The corollary to this observation is that the CO₂-SAG process improves recovery more than the miscible CO₂ process, inferring that reservoir pore microstructure heterogeneity is an indicator for the possible use of the CO₂-SAG process.

Figure 5 shows that there is also a linear relationship between the volume of injected CO₂ at BT and the fractal dimension. Viscous fingering is more developed in cores with strong heterogeneity, and leads to earlier CO₂ BT^[21]. At the same time, the interaction time between CO₂ and crude oil in the pores is shorter, and there is less dissolved CO₂ in the oil in the pores outside the preferential flow paths or CO₂-BT channels. By contrast, viscous fingering in the homogeneous core is weak and the amount of CO₂ injected before CO₂ BT is large, while more oil is produced, and there is a more pervasive and longer interaction time between CO₂ and the crude oil. In the CO₂-SAG process the CO₂ soaking process during CO₂-SAG flooding ensures that there is sufficient interaction between injected CO₂ and crude oil irrespective of the heterogeneity, leading to the CO₂-SAG process being less sensitive to pore-throat structure than miscible CO₂ flooding.

Figure 6 shows the CO₂-SAG process (combined green and red column) resulted in significantly higher recovery than the miscible CO₂ process (blue column), and that the improvement is better for the rocks with higher heterogeneity. This is shown by the proportion of the produced oil associated with soaking and secondary flooding (red column) to the total oil production in the homogeneous cores, H2 and H3, being 24% and 23%, respectively, while that for the more heterogeneous cores, H1 and H4, is 31% and 34%, respectively. Of course, it may be argued that the more homogeneous cores have already undergone production of a significant proportion of their producible oil in the initial CO₂ flooding (i.e., before gas breakthrough) and by consequence there is less left to be produced by the soaking and secondary flooding process. However, it is clear that the CO₂-SAG process provides improved oil recovery and is particularly effective in rocks with heterogeneous pore microstructures.

We have compared the improvement in oil recovery associated with the soaking and secondary flooding phases of the CO₂-SAG process for 4 populations of pores of different sizes, as shown in **Figure 7**. The improvement in oil recovery for the homogeneous cores (H2 and H3) increases with the pore radius, indicating that the larger the pores, the higher the potential for increased oil production. However, in the heterogeneous cores (H1 and H4), the pores with T₂ in the range 10-100 ms show the largest increase in oil production, indicating that the soaking process is allowing the production of oil from smaller pores which are by-passed by the miscible CO₂ flooding process^[24]. In the heterogeneous rocks, most of the oil in the largest pores (T₂>100 ms) is preferentially displaced before breakthrough because it is through these pores that the high permeability gas flow channels develop. By contrast, the smaller pores in the rock (T₂ <10 ms) provide smaller oil production from the rock with either process. This is due to the difficulty in sweeping the oil in these small pores from the rock. However, increasing soaking time might improve production from these smaller pores. Consequently, it may be said that the CO₂-SAG process operates primarily in the production of pores of a size which would normally be by-passed by the miscible CO₂ flood, and especially in heterogeneous rocks where the by-passing is more severe.

Table 4. Fractal dimensions of core pore-throat structure, oil RFs, permeability decline after flooding and asphaltene in produced oil (the original asphaltene in crude oil=1.32 wt%).

Flooding method	Core No.	<i>D</i> (unitless)	<i>S</i> _{oi} (%)	<i>k</i> _b (mD)	Oil RF at BT (%)	V _{CO2} at BT (PV)	Total oil RF (%)	<i>k</i> _d (%)	Decrease in asphaltene in produced oil (A _d wt%)
CO ₂ flooding	H1	2.706	51.4	0.713	-	-	43.1	13.1	0.61
	H2	2.622	62.9	0.742	-	-	57.7	9.6	0.53
	H3	2.596	65.5	0.769	-	-	61.9	7.5	0.47
	H4	2.748	42.3	0.734	-	-	39.6	14.2	0.66
CO ₂ -SAG flooding	H1	2.706	52.6	0.706	39.1	0.37	56.8	16.0	0.78
	H2	2.622	62.0	0.73	51	0.53	67.2	10.6	0.6
	H3	2.596	64.9	0.778	54.4	0.58	70.5	8.1	0.53
	H4	2.748	42.8	0.724	35.4	0.28	53.2	17.8	0.89

Notes: *D*: Fractal dimensions of core pore-throat structure, *S*_{oi}: oil saturation of cores before flooding, oil RF at BT: oil recovery factor before CO₂ BT, V_{CO2} at BT: the volume of injected CO₂ before CO₂ BT, *k*_b: core permeability before flooding, *k*_d: permeability decline after flooding.

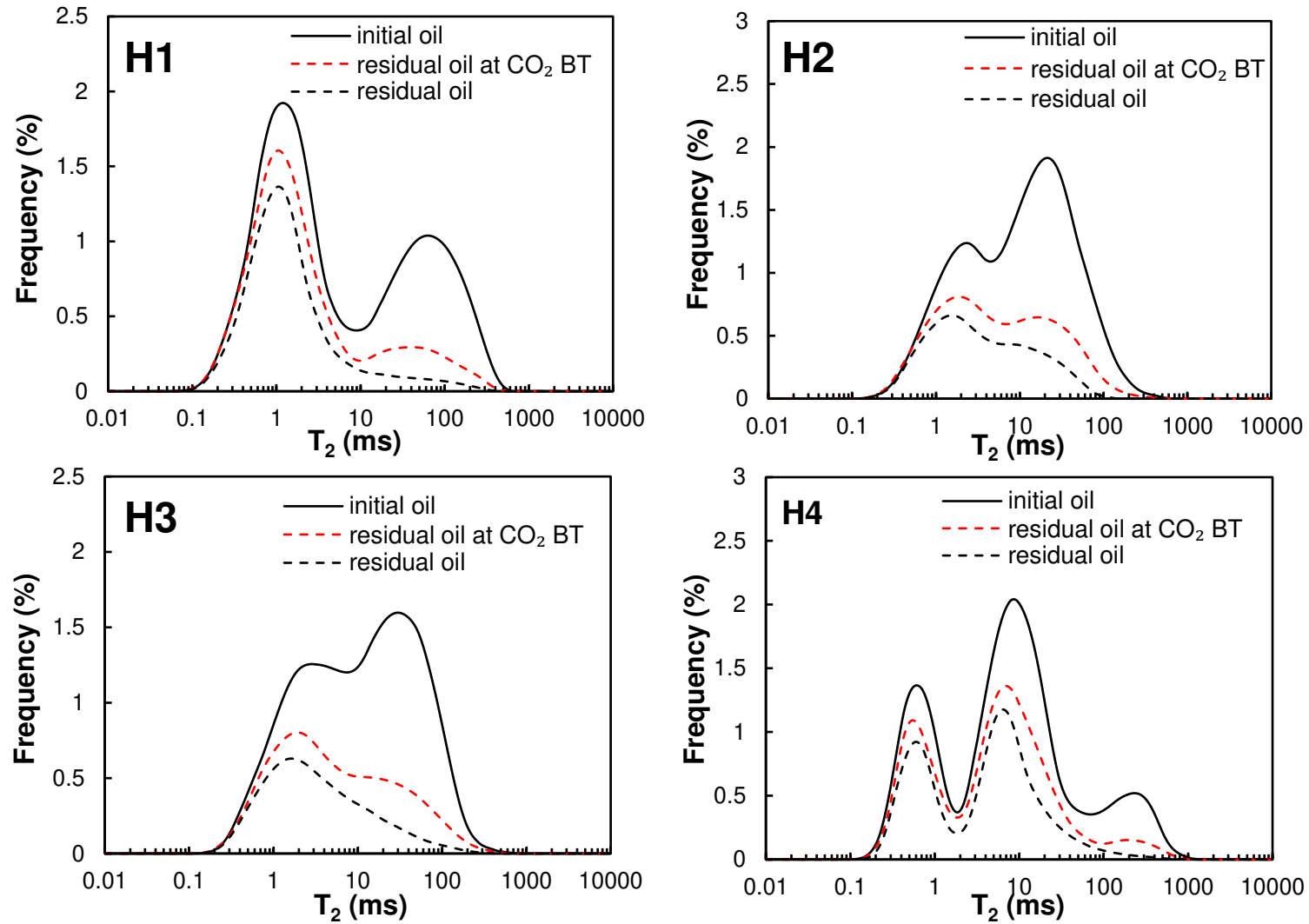


Figure 3. The initial oil distribution in cores before flooding, residual oil at CO_2 BT and residual oil after flooding by NMR T_2 spectra.

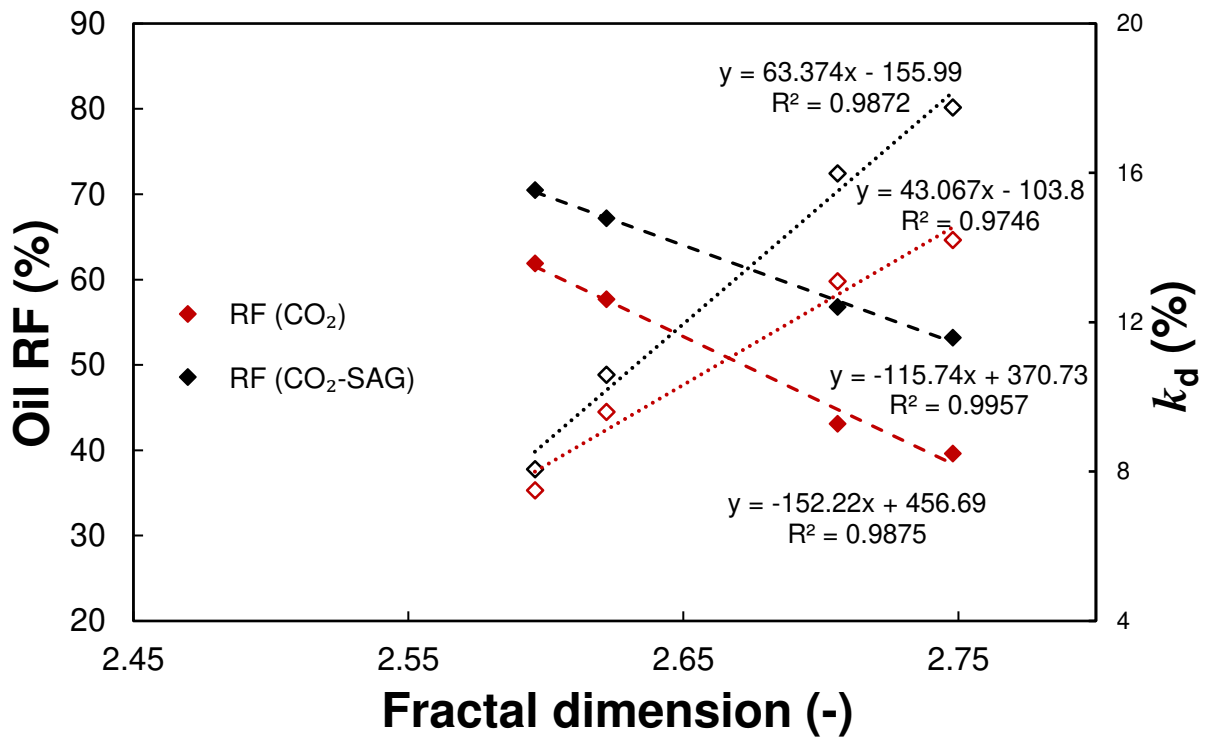


Figure 4. Oil RF and k_d as a function of fractal dimension after flooding for both the CO_2 -SAG flooding presented in this paper (in black) and for miscible CO_2 flooding^[13] (in red).

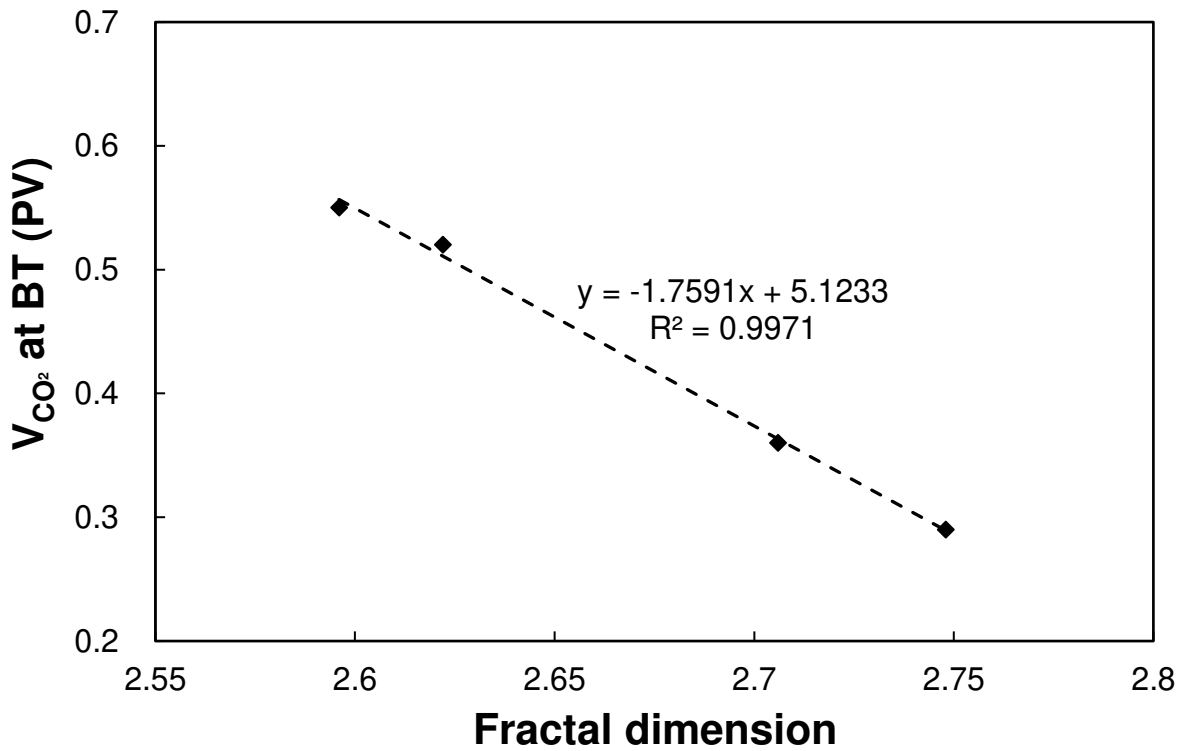


Figure 5. The volume of injected CO_2 before CO_2 BT versus fractal dimension.

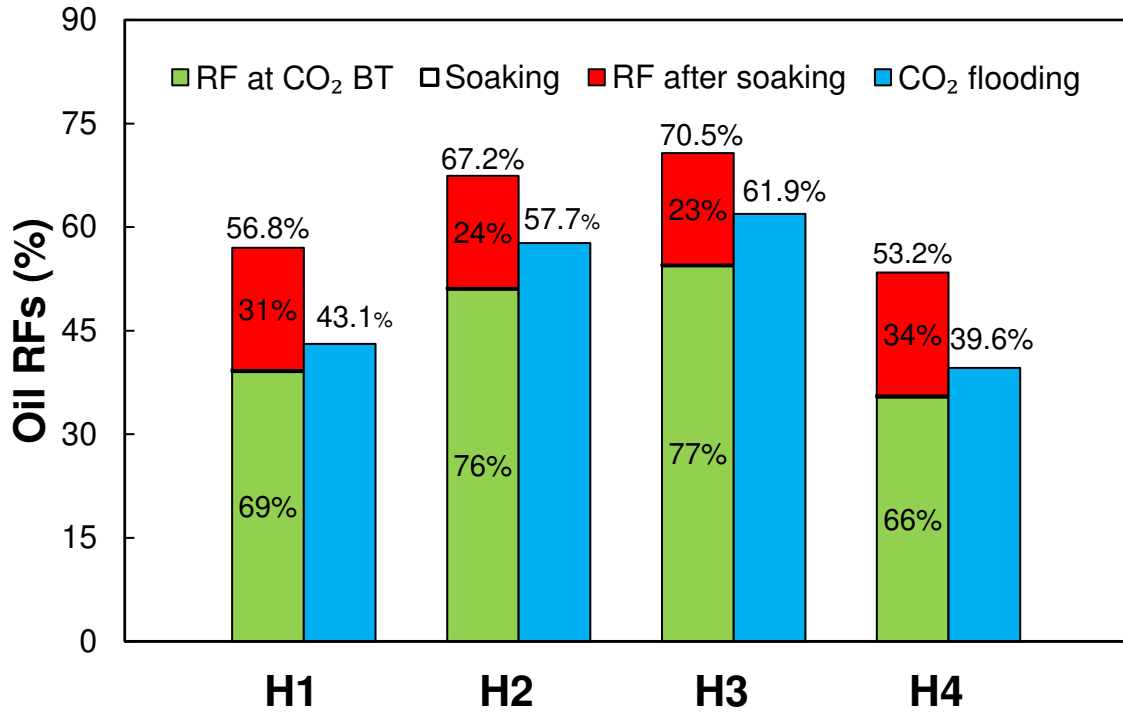


Figure 6. Oil RFs at CO₂ BT (green) and after soaking and secondary flooding (red) during CO₂-SAG flooding (this work), compared with the total oil RFs after miscible CO₂ flooding^[13] (blue).

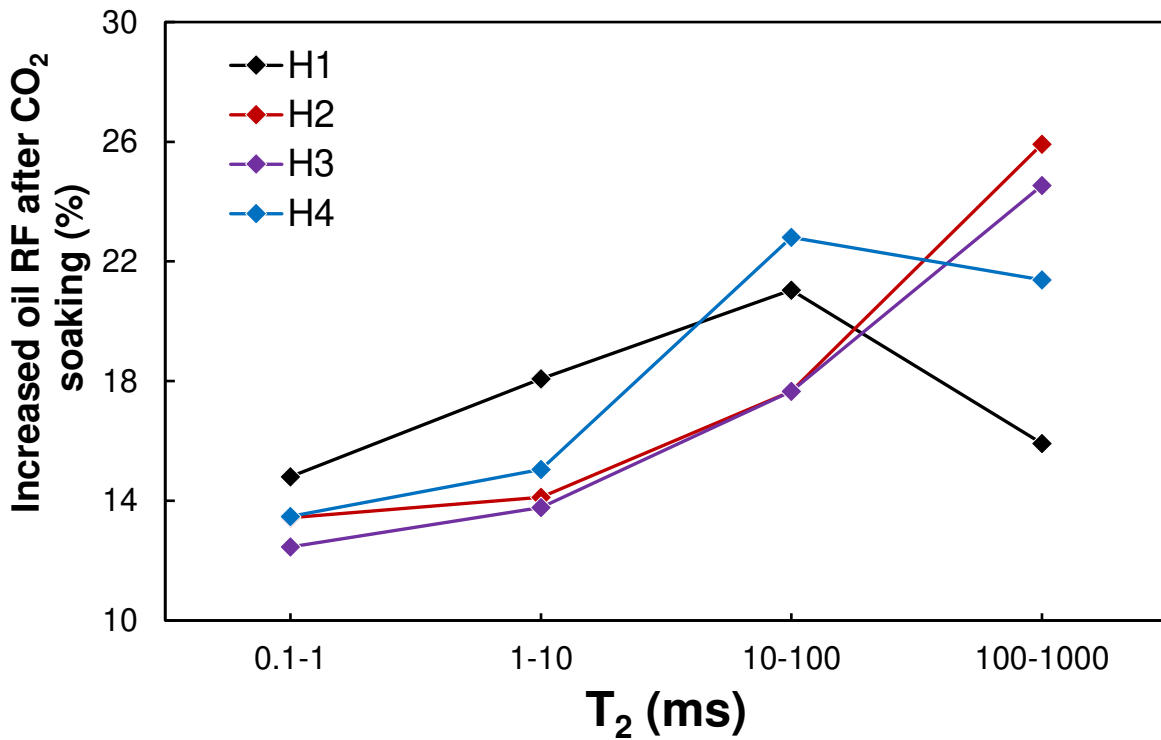


Figure 7. Increase in oil RF after soaking in different size of pores comparing the RFs at CO₂ BT with total RFs after CO₂-SAG flooding.

Pressure decay in the CO₂-soaking process

The CO₂ trapped in pores of cores is gradually dissolved in the nearby crude oil, thus causing the pressure of the fluid in the rock pores to decay, as shown in [Figure 8](#). Here, the decay pressure is the average value of the gas pressures measured at the inlet and outlet faces of the core. As CO₂ BT has already occurred, and there is good connectivity between the inlet and outlet through high flow CO₂ BT channels^[29], the differential pressures are relatively small. The measured average pressure inside the core initially reduces rapidly, reaching a stable value as time progresses. The decrease is approximately exponential because it arises from a process whereby dissolution of gas in oil is controlled by the amount of gas already dissolved in the oil. As more gas dissolves in the oil occupying a given pore space the process of dissolution becomes steadily less efficient until gas dissolution ceases and the exponential pressure decay levels off^[30]. The fine structure of the pressure decays is probably related to the accessibility of oil by the gas. We hypothesise that the initial rapid decay is due to dissolution in oil which is in direct contact with the CO₂, while later decay depends on the CO₂ being in contact with oil which is not saturated with oil yet, or on gas diffusion processes within the oil.

The cores with greater homogeneity of pore microstructure show faster pressure decays in the early rapid decay stage (H3>H2>H1>H4). This shows that the CO₂ trapped in the homogeneous core is quickly dissolved in the residual oil. For these cores, the total CO₂-SAG flooding time can be shortened and subsequent CO₂ flooding can be performed earlier. This is due to the relatively large swept volume and pervasive distribution of CO₂ at CO₂ BT in H2 and H3, which maximizes contact between the CO₂ and the crude oil. Cores with more homogeneous pore structures also tended to have higher final pressures. This is primarily due to there being a higher and more pervasive gas saturation in the core at the start of the soaking process due to the miscible CO₂ flooding process prior to BT being more efficient in these rocks.

We observe that as the heterogeneity of the pore microstructure increases the final pressure is also controlled by the dissolution of CO₂ into the brine or crude oil in smaller pores. The fluid in these pores has a very low mobility due to small pore-throats which connect them. Furthermore, the fluid in these small pores is more likely to be brine, with these small pores exhibiting strong wetness to water. While the CO₂ still dissolves in whatever oil is present, most of the fluid is water, in which CO₂ can also dissolve. However, under the same pressure and temperature conditions, the solubility of CO₂ in brine is lower than the solubility of CO₂

in crude oil. The disparity provides a supplementary reason for the final pressures in heterogeneous cores is observed to be greater than those for homogeneous samples. However, it also has another important outcome. The imposition of a long CO₂ soaking time will cause CO₂ to begin to dissolve into the brine, reducing its viscosity and causing a portion of it to become mobile. The newly mobile water can then be displaced by subsequent CO₂ flooding. The efficacy of CO₂ transmission may then be reduced because the newly mobile water impedes its flow^[31]. Overall, therefore, slow pressure decay associated with long soaking times impedes crude oil production and increases the production cost of the oil field.

In order to save time and improve efficiency, the soaking time needs to be curtailed in order to avoid the slowly decaying pressure phase. We choose an optimal time point (T_c) which is designed to take advantage of the dissolution of CO₂ in oil, when the pressure decays quickly, but avoid the dissolution of CO₂ in formation water, which is associated with later slow pressure decay. The core is subjected to a soaking phase for a period given by T_c , after which secondary miscible CO₂ injection is carried out for the displacement of the mobilised oil. The optimal time point is taken to occur when the pressure decay rate is less than 0.01 MPa/min (Figure 9).

It is observed for our cores that not only the value of T_c increases with the fractal dimension of pore-throat structure, but that the pressure decays by more than 80% of the total pressure drop during soaking process by the time T_c is reached. These observations indicate that during the rapid pressure decay stage, the dissolution of CO₂ in crude oil is sufficient enough to ensure the efficiency of subsequent CO₂ flooding, and the selection of T_c is reasonable. It is worth noting that although the pressure decay curves of H2 and H3 reached a pressure decay rate of less than 0.01 MPa/min earlier than those of H1 and H4, the magnitude of the pressure decay was smaller (around 7%). This is because the transition between the rapid decay period and the steady decay period of the pressure decay curves of H1 and H4 is relatively smooth, and the differences between the two stages of H2 and H3 are more obvious. Consequently, in subsequent experimental studies, we do not have to wait until the pressure has completely stopped declining before starting subsequent CO₂ flooding. It is worth noting that our selected criterion for defining when T_c occurs is not likely to apply equally to all reservoirs. Instead, it would be worthwhile defining a new criterion for T_c for individual reservoirs, based on its effect on ultimate oil RF.

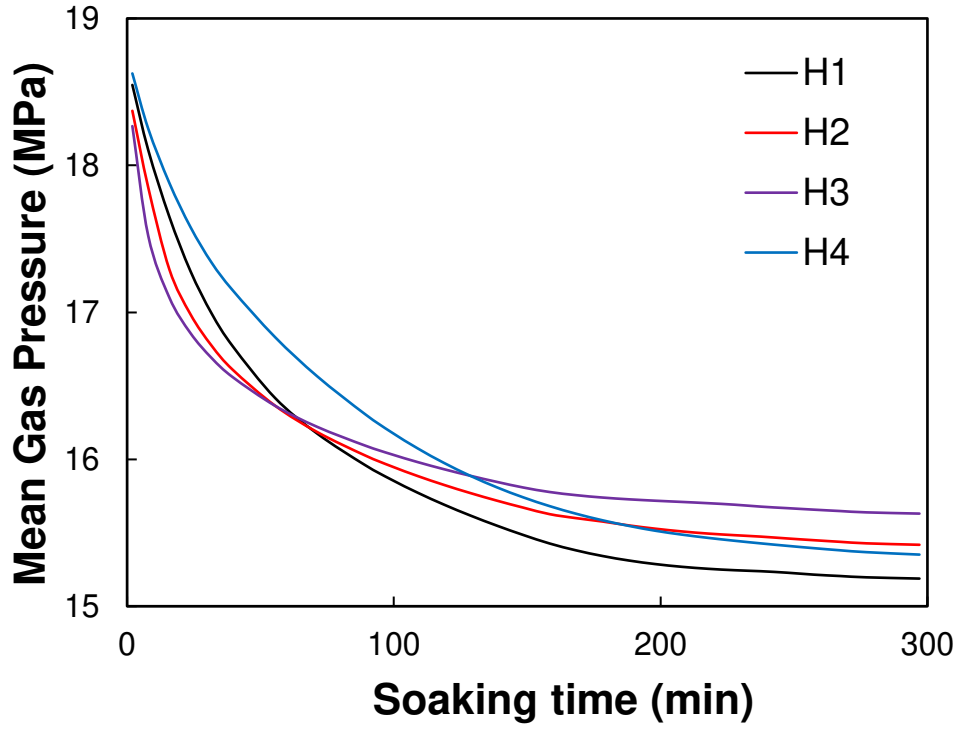


Figure 8. Mean gas pressure in the core plugs as a function of soaking time.

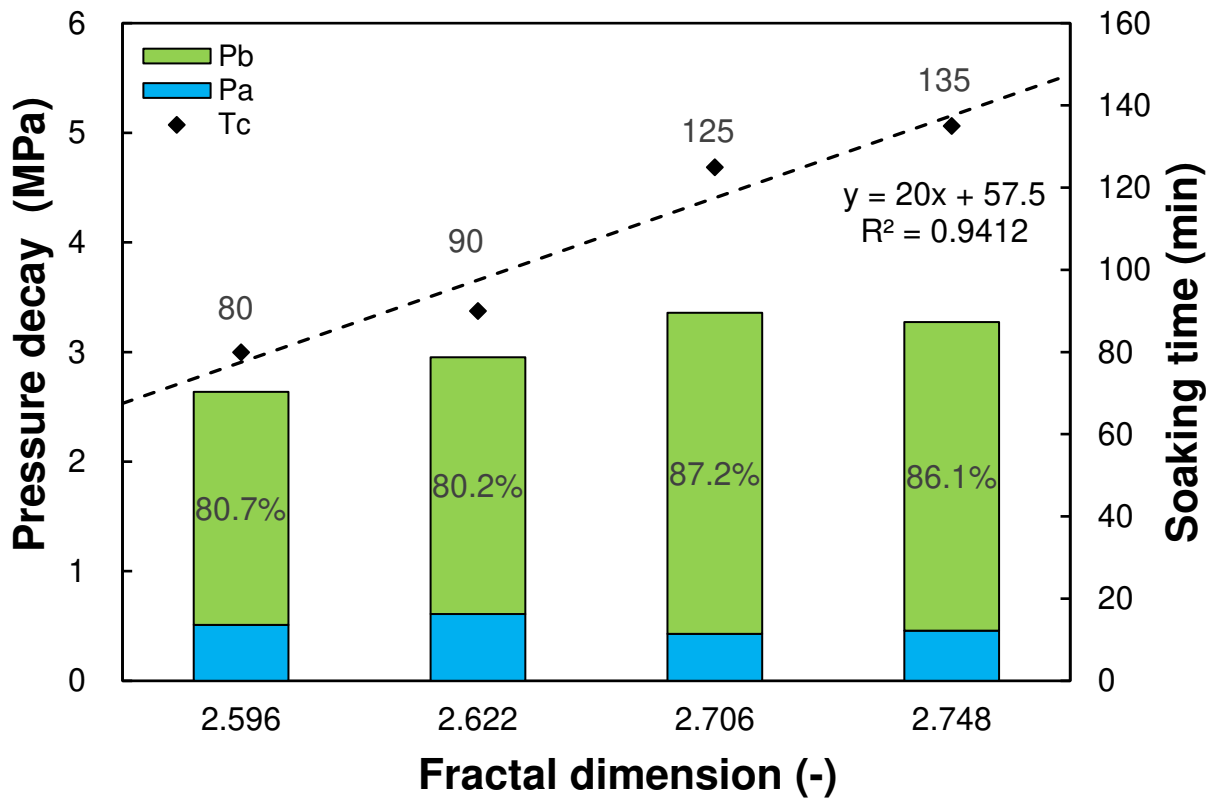


Figure 9. The pressure decay (columns) and soaking time (symbols and fitted line) as a function of fractal dimension during pressure decay. T_c is the optimal soaking time point (min); P_b is the pressure drop before T_c (MPa); P_a is the pressure drop after T_c (MPa).

Permeability damage and asphaltene precipitation

We have compared the permeability before CO₂-SAG flooding with that after flooding, together with the asphaltene content in the original oil and the produced oil. The process of flooding leads to a decrease in core permeability (k_d) and a decrease in asphaltene content in the produced oil (A_d), which is shown in [Table 4](#). Permeability damage can be caused by (i) CO₂–brine–rock interactions, and (ii) asphaltene precipitation.

The first of these two process has a negligible effect on permeability, as shown by the results of simple miscible CO₂ flooding experiments on these cores^[12]. This insignificant effect has been attributed to (i) the limited contact area between CO₂, brine and rock, and (ii) the core-flooding time not being conducive to CO₂–brine–rock interactions. For water-wet rock matrices, brine is distributed in small pores or on the surface of minerals in the form of thin film, where the injected CO₂ cannot easily access. Consequently, there is little formation of carbonated brine. For oil-wet surfaces, CO₂ does carbonate the brine, but the oil film on the surface of minerals hinders the contact between carbonated water and minerals. Hence, CO₂–brine–rock interactions is negligible irrespective of the wettability of the reservoir rock. In addition, whatever CO₂–brine–rock contact is possible, interaction is limited by the core-flooding time being too short for significant damage to take place^[16,32].

By contrast, the second process, asphaltene precipitation, does have a significant effect on permeability. Our observations of decreases in core permeability together with a reduction in the amount of asphaltene in the produced oil compared to the initial oil suggests strongly that asphaltenes have precipitated in the cores during CO₂-SAG flooding, and are the cause of the permeability degradation. Small asphaltene particles precipitate from crude oil, gradually growing in size during the process of migration with the oil through the rocks. When the size of the asphaltene particles approach or exceed the size of the pore-throats, the particles become trapped, forming blockages that reduce the overall connectivity of the rock, and hence reduce the permeability of the reservoir. At the same time, asphaltene precipitates are also continuously adsorbed on the surfaces of rock minerals, causing the pores and pore-throats to gradually decrease in size, and making asphaltene precipitates more likely to block the pore-throats. In addition, the surface adsorption of these asphaltene precipitates also causes changes in rock wettability.

In this work, the permeabilities of the cores were measured before flooding, immediately after the flooding, following standard core cleaning procedures, and finally after the cores have been cleaned to remove all asphaltene precipitates. When this was done, it was noted that the restored permeability values were only slightly different from the pre-flooding permeabilities ($\pm 1.7\%$), while the porosities also returned to approximately their pre-flooding values ($\pm 1.3\%$). Consequently, we have been able to observe the effect of asphaltene precipitation on permeability as a result of flooding with CO_2 , as well as to restore the original porosity and permeability when the precipitated asphaltene was removed. The corollary is that damage to permeability of cores subsequent to CO_2 -SAG core-flooding observed in this paper is primarily due to asphaltene precipitation.

In this work, both k_d and A_d after CO_2 -SAG flooding were found to be larger than those after simple miscible CO_2 flooding, namely 0.6-3.6% and 0.06-0.23wt%, respectively. We have attributed the increased permeability damage and loss of asphaltene from the oil to enhanced interaction between CO_2 and the crude oil in the pores, and the consequent additional precipitation of asphaltenes, during the soaking phase of the CO_2 -SAG flooding. **Figure 10** shows that there is a linear relationship between decreased permeability (k_d) and reduction in asphaltene content (A_d) versus oil recovery factor.

Large oil RFs are expected to correspond to large decreases in permeability, because larger CO_2 sweep volumes and high CO_2 flooding efficiency implies more asphaltene precipitation^[19]. Indeed, **Figure 4** and **Figure 10** show that the k_d decreases with increasing oil RF, but also increases with fractal dimension. Cores H2 and H3 with homogeneous pore-throat structures have large oil RFs with small k_d . This may be attributed to the observation that cores with homogeneous pore-throat structure may be relatively insensitive to permeability damage caused by asphaltene precipitation, cores with more homogeneous pore-throat structure resist damage to permeability by asphaltene precipitation compared to heterogeneous cores. In the heterogeneous cores, the complexity of the pore and pore-throat structure ensures that CO_2 is trapped and remains in contact with oil occupying small pores without oil being produced^[33-34]. Consequently, there is a larger decrease in asphaltene content in the produced oil because more asphaltene precipitates in the rock. Furthermore, the asphaltene is precipitated in small pores and pore-throats where it has a greater potential for clogging flow pathways. In the homogeneous cores, more crude oil in the pores is driven out by injected CO_2 , and a large amount of asphaltene precipitation is also generated in the process. However part of the

precipitation is carried out of the cores with the crude oil, and less asphaltene precipitate remains in the cores. In addition, even with the same scale of asphaltene precipitation in the cores, the pore-throat structure of the homogeneous core is less affected by asphaltene precipitation, and the permeability decline is relatively smaller, indicating that the homogeneous pore-throat structure will weaken the effect of asphaltene precipitation on the permeability decline.

It is worthwhile noting that k_d and A_d at any given value of RF are larger after CO₂-SAG flooding than after simple miscible CO₂ flooding (Figure 10). The process of CO₂ soaking reduces the viscosity of crude oil in smaller pores and weakens the viscous fingering effect, which makes the crude oil in smaller pores easier to displace^[24,35]. Moreover, the CO₂ soaking causes severe asphaltene precipitation in the pores resulting in more blockage at more pores and throats. In addition, the larger gradient of the slope of k_d as a function of oil RF in Figure 10 indicates that the degree of permeability damage during CO₂-SAG flooding is more sensitive to variations in oil RF than for simple miscible CO₂ flooding.

The value of A_d in produced oil can represent the situation of asphaltene precipitation in cores to some extent during flooding. A large A_d corresponds to a large decrease in permeability (Figure 11); the more asphaltene particles precipitate in the pores, the greater the probability that the pores will be blocked as a result of particle migration^[36]. However, for the same value of A_d , the permeability after CO₂-SAG flooding decreases less, because there is no CO₂ displacement during the soaking process, resulting in more asphaltene adsorption on pores rather than blockage at pore-throats, and consequently less damage to permeability. Figure 11 allows the permeability damage to a reservoir by asphaltene precipitation from each of the two flooding methods to be roughly estimated.

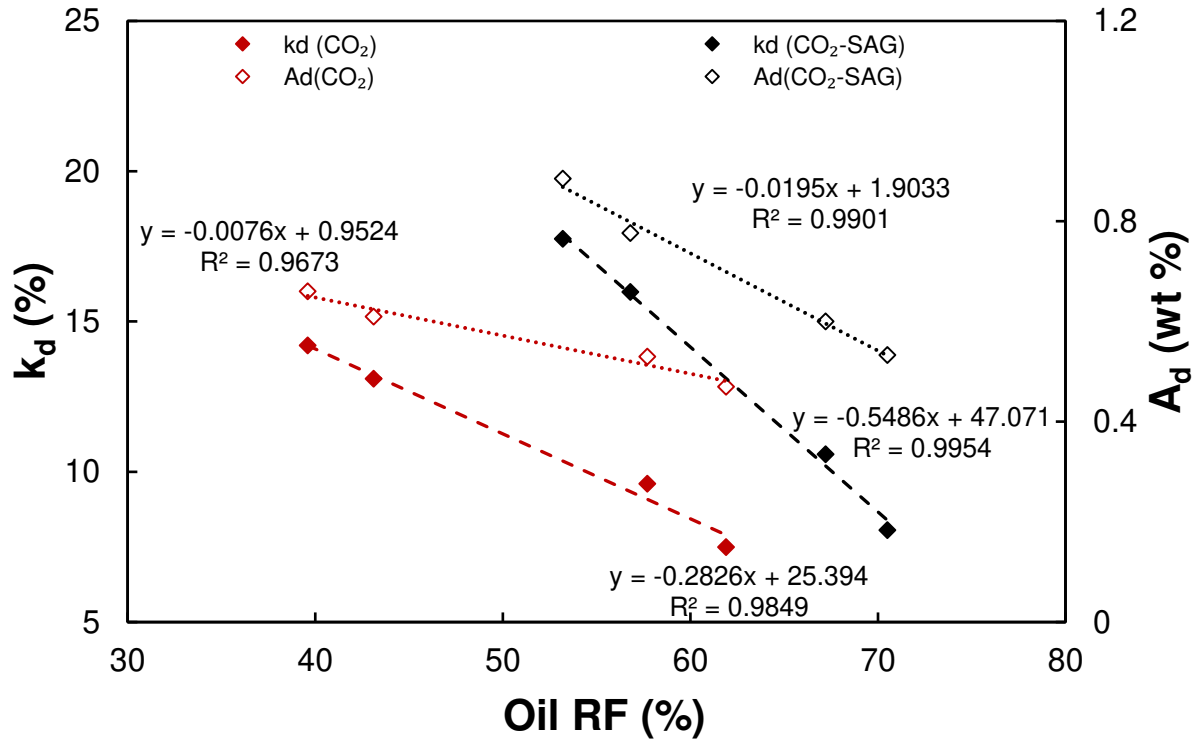


Figure 10. k_d and A_d as a function of oil RF after flooding. k_d is the decrease in permeability caused by CO_2 -SAG flooding and A_d is the decline of asphaltene content in the produced oil compared with initial oil for both the CO_2 -SAG flooding presented in this paper (in black) and for simple miscible CO_2 flooding^[13] (in red).

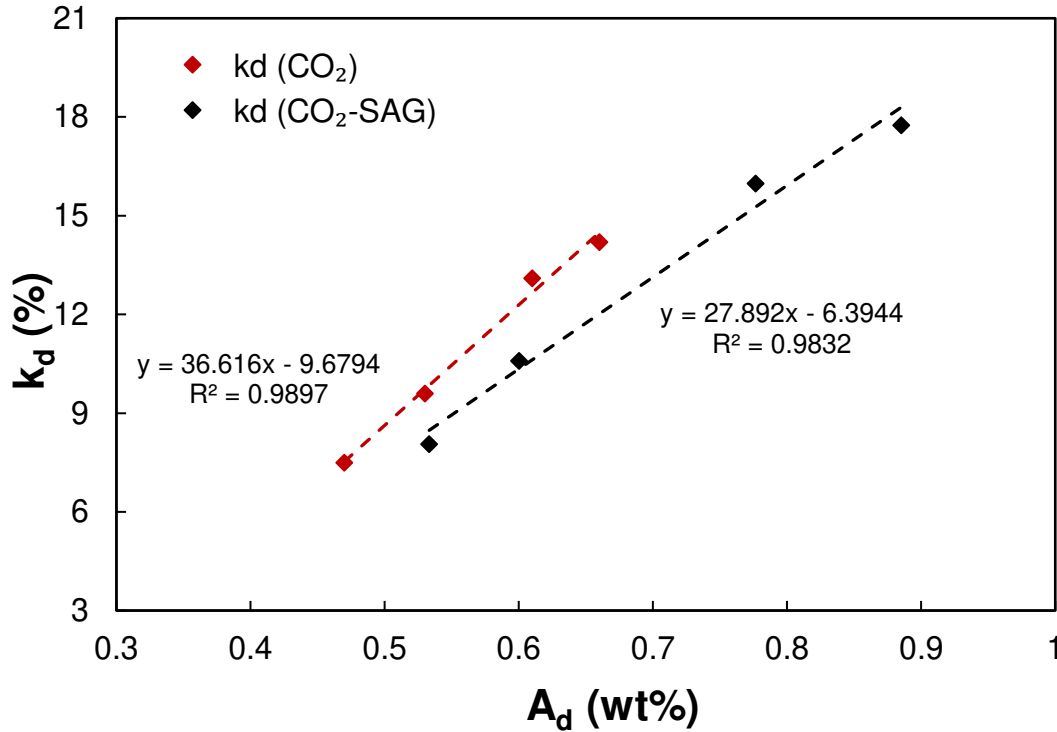


Figure 11. k_d as a function of A_d after flooding for both the CO_2 -SAG flooding presented in this paper (in black) and for miscible CO_2 flooding^[13] (in red).

Changes in Recovery Factors and Permeability

We have defined two parameters to allow the more detailed comparison of the simple miscible CO₂ flooding process with the CO₂-SAG process. The first expresses the percentage increase in recovery factor as $RF_i = (RF_{CO_2-SAG} - RF_{CO_2}) / RF_{CO_2} \times 100\%$, while the second expresses the percentage difference in permeability decline (permeability damage) as $k_{di} = (k_{d-CO_2-SAG} - k_{d-CO_2}) / k_{d-CO_2} \times 100\%$. Large values of RF_i indicate an advantage of the CO₂-SAG flooding process over the simple miscible CO₂ flooding process because more oil is produced, while large values of k_{di} indicate a disadvantage of the CO₂-SAG flooding process over the simple miscible CO₂ flooding process because there is greater permeability damage to the reservoir.

Figure 12 shows that both RF_i and k_{di} are related linearly to the fractal dimension. For heterogeneous rocks the CO₂-SAG flooding process leads to better recovery factors but does so at the expense of greater formation permeability damage than would be the case if simple miscible CO₂ flooding had been used. In such cores (i) the interaction time between CO₂ and crude oil is short because there occurs an earlier CO₂ BT caused by viscous fingering, and (ii) the CO₂ soaking phase alleviates the insufficient dissolution of CO₂ in the crude oil, which is more serious in cores with strong heterogeneous pore-throat structures. Consequentially, compared to simple miscible CO₂ flooding, CO₂-SAG flooding can significantly improve the oil RFs of cores with poor pore-throat structure and weaken the effect of pore-throat structure on oil RFs. It should be noted that, although the CO₂-SAG flooding causes a greater decrease in permeability than the simple miscible CO₂ flooding, the amplitude of the effect is smaller than the corresponding increase in recovery factor, which indicates that CO₂-SAG flooding is a relatively efficient method with low damage to the reservoir. This may be observed most effectively by plotting the ratio of permeability decline (damage) to recovery factor, $k_{dp} = k_d / RF$, for each flooding process against the fractal dimension of each core, as in Figure 13. The parameter k_{dp} represents the permeability decrease (damage) per unit increase in recovery factor, where small values are better than large values as they represent smaller degrees of permeability damage per increase in produced oil. Figure 13 shows that the values of k_{dp} have good linear relationship with the fractal dimension of pore-throat structure for both flooding processes. In other words, the more heterogeneous the pore-throat structure is, the more severe the damage to the permeability after flooding with the same oil RF. Importantly, the k_{dp} curve for CO₂-SAG flooding is lower than that of simple miscible CO₂ flooding for each fractal dimension, which indicates that the CO₂-SAG flooding process causes less permeability

damage per increase in recovery factor than the simple miscible CO₂ flooding process for both homogeneous and heterogeneous cores.

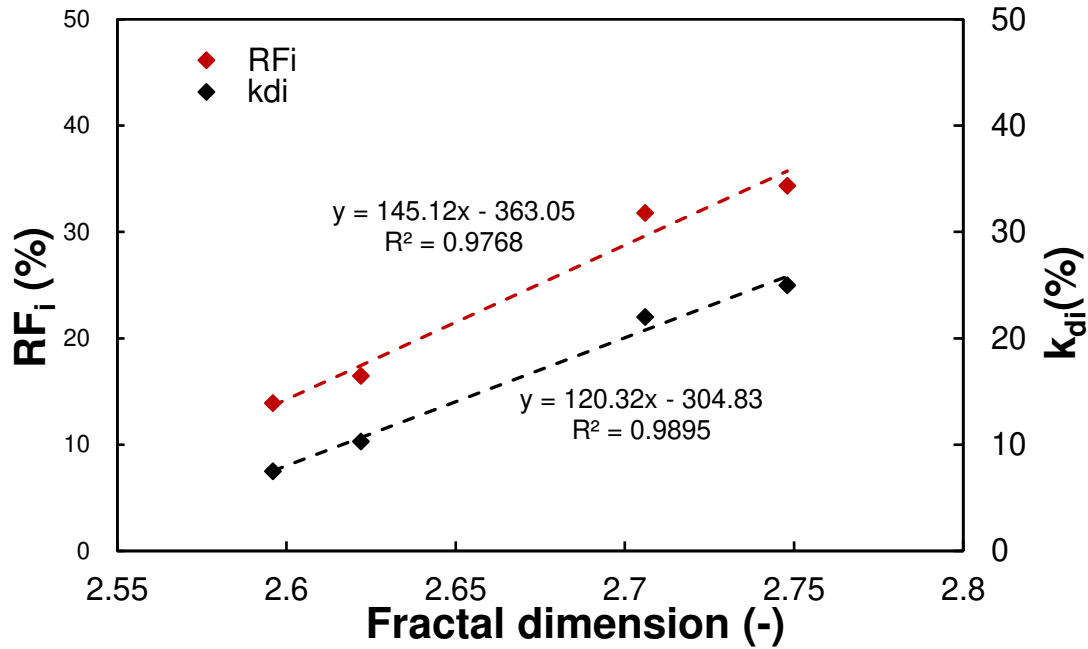


Figure 12. The increase in oil RF and the increase in k_d as a function of fractal dimension for both the CO₂-SAG flooding presented in this paper (in black) and for miscible CO₂ flooding^[13] (in red). Increase in oil RF; $RF_i = (RF_{CO_2-SAG} - RF_{CO_2}) / RF_{CO_2} \times 100\%$. Increase in oil k_d , $k_{di} = (k_{d-CO_2-SAG} - k_{d-CO_2}) / k_{d-CO_2} \times 100\%$.

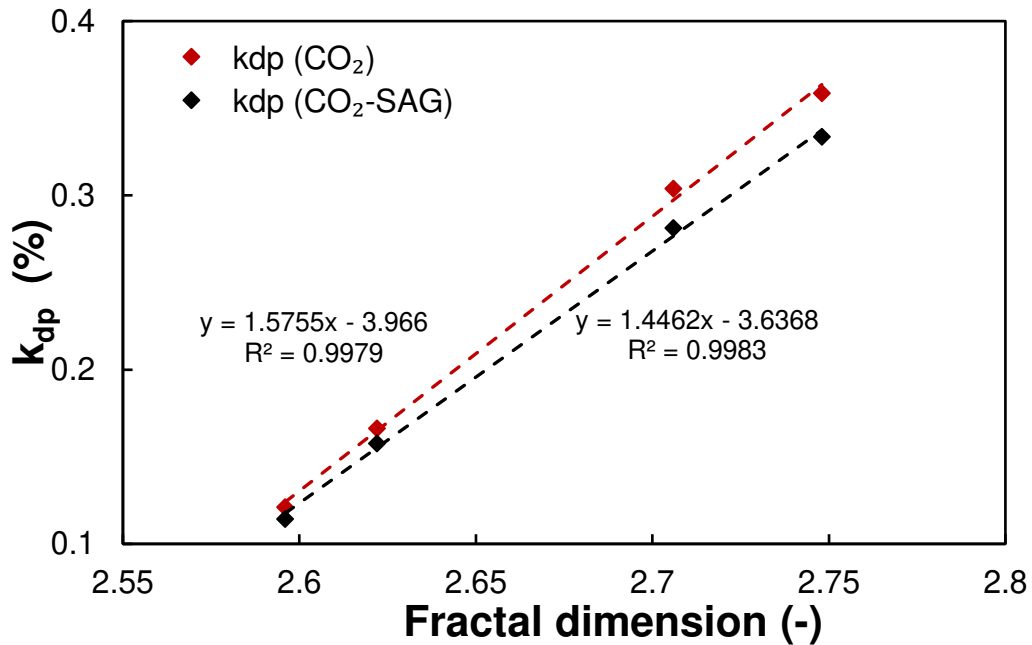


Figure 13. The permeability decline by per unit percentage change in oil RF, $k_{dp} = k_d / RF$, as a function of fractal dimension for both the CO₂-SAG flooding presented in this paper (in black) and for miscible CO₂ flooding^[13].

Variation in Brine Saturation

The T_2 spectra given in [Figure 14](#) show the distribution of brine before flooding and re-saturated with brine after flooding. It is worth noting that before being re-saturated with brine, the core was cleaned and aged in brine only with adsorbed asphaltene precipitation trapped in the pores. The variation in brine saturation S_{wv} was calculated according to $S_{wv} = S_{wb} - S_{wa}$, where S_{wb} is the brine saturation before flooding (the solid line in [Figure 14](#)), and S_{wa} is the brine re-saturation after flooding (the dotted line in [Figure 14](#)). Consequently, the S_{wv} parameter represents the degree of change in the brine saturation of the cores due to the flooding.

Brine re-saturation after flooding is affected by two factors; (i) blockage of the pore-throats, and (ii) changes to the wettability of cores^[37]. In the first case, pores cannot be fully re-saturated with brine when pore-throats are blocked due to the migration of asphaltene precipitation particles^[38]. Consequently, the signal amplitude on the T_2 spectrum of brine in these pores shows significant decline after re-saturation. In the second case, the asphaltene precipitate adheres to the surface of the pores, making the asphaltene precipitated rocks more oil-wet. Both of these factors play a role in resisting water re-saturation, and hence increase the value of S_{wv} .

Although it might be expected that both processes would affect smaller pores and their connecting pore-throats disproportionately more than they would affect larger pores and pore-throats, this is not the case. We propose the following hypothesis. Asphaltene precipitation and wettability change only happens where oil has been displaced by CO_2 before BT. This occurs in larger pores which are well-connected by larger pore-throats and become the gas flow channels taken by the CO_2 at breakthrough. Furthermore, flow of asphaltene particles occurs predominantly in the same gas flow channels immediately ahead of the advancing CO_2 front. Consequently, one would expect wettability change to occur in the larger pores making up the gas flow channels and blockage to occur in those smaller and medium sized pore-throats leading off from the main flow. The blockage mechanism could, in some highly heterogeneous rocks, provide a mechanism for stopping CO_2 flow into pores through medium and smaller pore-throats. [Figure 14](#) shows that the reduction in water saturation caused by the flooding does take place preferentially in the larger pores for the three most heterogeneous of the four cores, which supports our hypothesis.

Figures 15 and Figure 16 show the relationships of S_{wv} with oil RF and fractal dimension, respectively. These figures include the data from all four cores when subjected to both simple miscible CO₂ flooding and CO₂-SAG flooding.

In Figure 15, homogeneous cores exhibit a larger reduction in water saturation than more heterogeneous cores for both simple miscible CO₂ flooding and CO₂-SAG flooding. Core-by-core comparison of Figure 15 with Figure 14 shows that the three cores for which the value of S_{wv} is highest all display water saturation reductions preferentially in the largest pores compared to the smaller pores. Both of these observations are consistent with our previous hypothesis for CO₂-SAG flooding, which is equally valid in the case of simple miscible CO₂ flooding.

In Figure 16, large values of S_{wv} are associated with high oil RFs. However, Figure 9 has already shown that high oil RF also corresponds to small k_d values (representing less blockage at pores and throats) after flooding. Consequently, we may infer that the variation in wettability has a more significant effect on water saturation than blockage at pores and throats, and consequently plays a major role in determining the value of S_{wv} . It is worth noting that this changes in wettability refers to the changes in the overall wettability of the whole rock, mainly referring to the wettability of the pore surface inside the core. Measurements of contact angle only reflect the wettability of the core surface being tested rather than the average wettability for the whole rock. Consequently, we did not perform the contact angle tests to study the changes in wettability in this work. Instead, the value of S_{wv} can represent changes in overall rock wettability in this paper. Furthermore, the value of S_{wv} after CO₂-SAG flooding is higher than that after simple miscible CO₂ flooding, which may be due to greater and more extensive asphaltene precipitation occurring during the CO₂ soaking stage of the CO₂-SAG process, implying that the CO₂-SAG process should lead to greater overall changes in wettability compared with simple miscible CO₂ flooding.

In addition, the range of difference in S_{wv} between four cores after CO₂-SAG flooding (1.6-1.8%) is smaller than that after CO₂ flooding (1.4-3%), this means that the range of S_{wv} values between the four cores after CO₂-SAG flooding is smaller than that of simple miscible CO₂ flooding, and hence CO₂-SAG flooding can weaken the effect of core pore-throat heterogeneity. This is possibly due to the greater opportunity that CO₂ has to interact with crude oil in pores of more varied morphology in the heterogeneous cores during the CO₂ soaking stage of the flooding process.

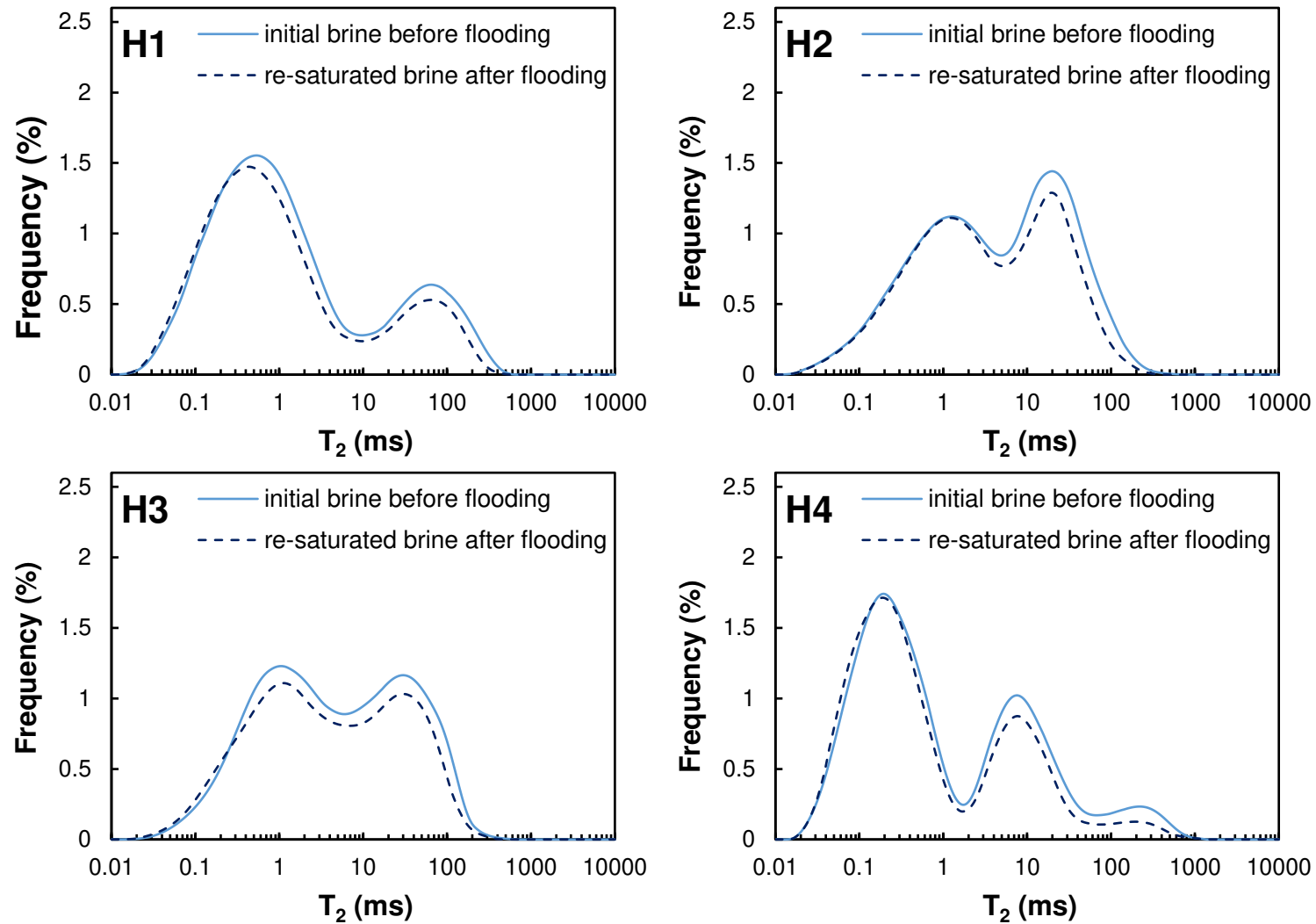


Figure 14. NMR T_2 spectra of brine distribution in cores showing initial brine before flooding and the restores saturations after flooding and cleaning.

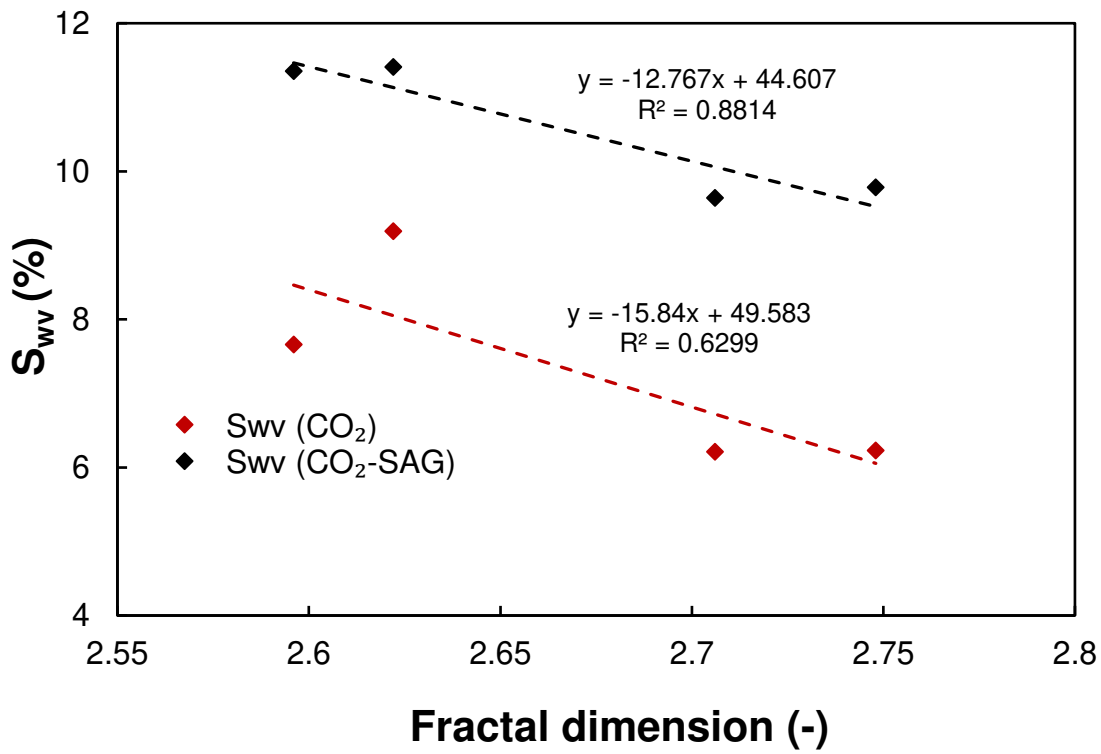


Figure 15. S_{wv} as a function of fractal dimension for both the CO₂-SAG flooding presented in this paper (in black) and for miscible CO₂ flooding^[13] (in red).

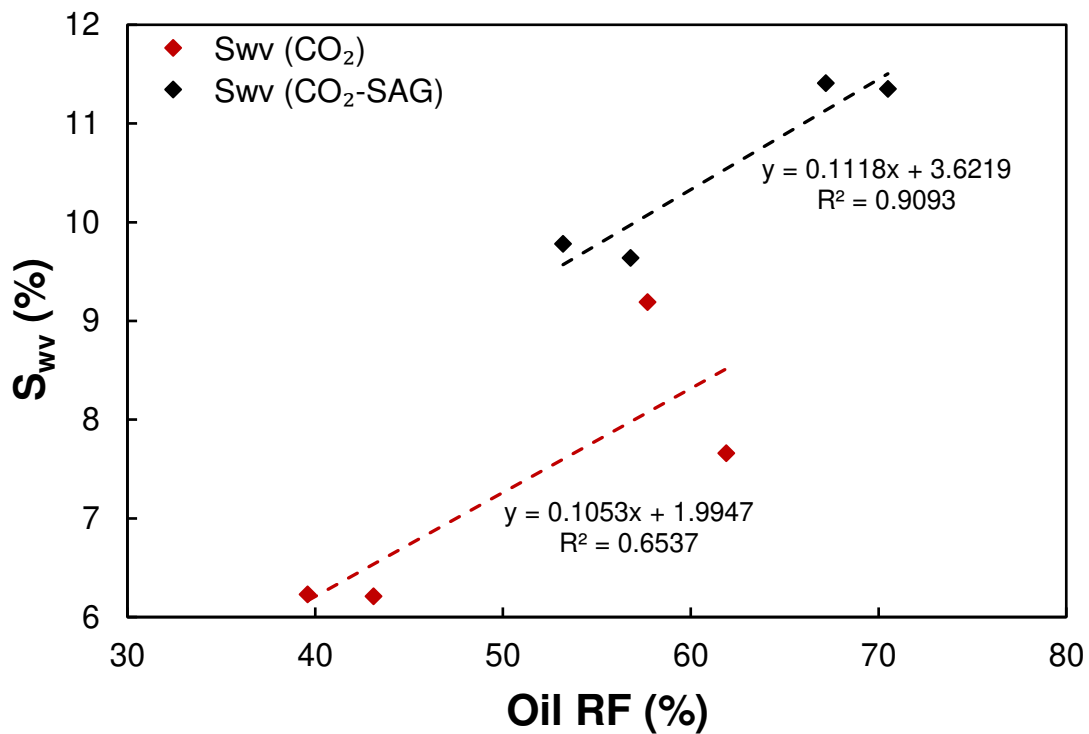


Figure 16. S_{wv} as a function of oil RF for both the CO₂-SAG flooding presented in this paper (in black) and for miscible CO₂ flooding^[13] (in red).

Comparison of the miscible CO₂ flooding process with the CO₂-SAG process

Figure 17 shows k_{di} , RF_i , S_{wvi} and A_{di} , which represent the difference in k_d , RF , S_{wv} and A_d between CO₂-SAG flooding and simple miscible CO₂ flooding. The S_{wvi} has the largest value, indicating that the CO₂ soaking stage has a large effect on wettability. Clearly, the wettability changes caused by soaking cannot be ignored, and necessary measures must be taken to suppress asphaltene precipitation during the soaking stage. The parameter k_{di} has the smallest value, much smaller than S_{wvi} , indicating that the effect of CO₂ soaking on k_d is relatively weak, (i) because migration of asphaltene particles does not occur during the CO₂ soaking process, (ii) the asphaltene precipitation in the smaller pores increases due to CO₂ soaking process, and (iii) in the subsequent CO₂ injection process, the probability of particle migration in the smaller pore-throat is also small. Whilst the possibility of adsorption on the pore surface is more significant, this means less probability of pore-throat blockage and greater change in wettability^[39]. The RF_i is higher than the k_{di} and A_{di} , indicating that CO₂-SAG flooding did not increase k_d and A_d significantly, while increasing the oil RF . In summary, higher oil RF s with significantly less damage to cores indicates that CO₂-SAG flooding is a reliable method for improving oil RF s in general and particularly in heterogeneous rocks.

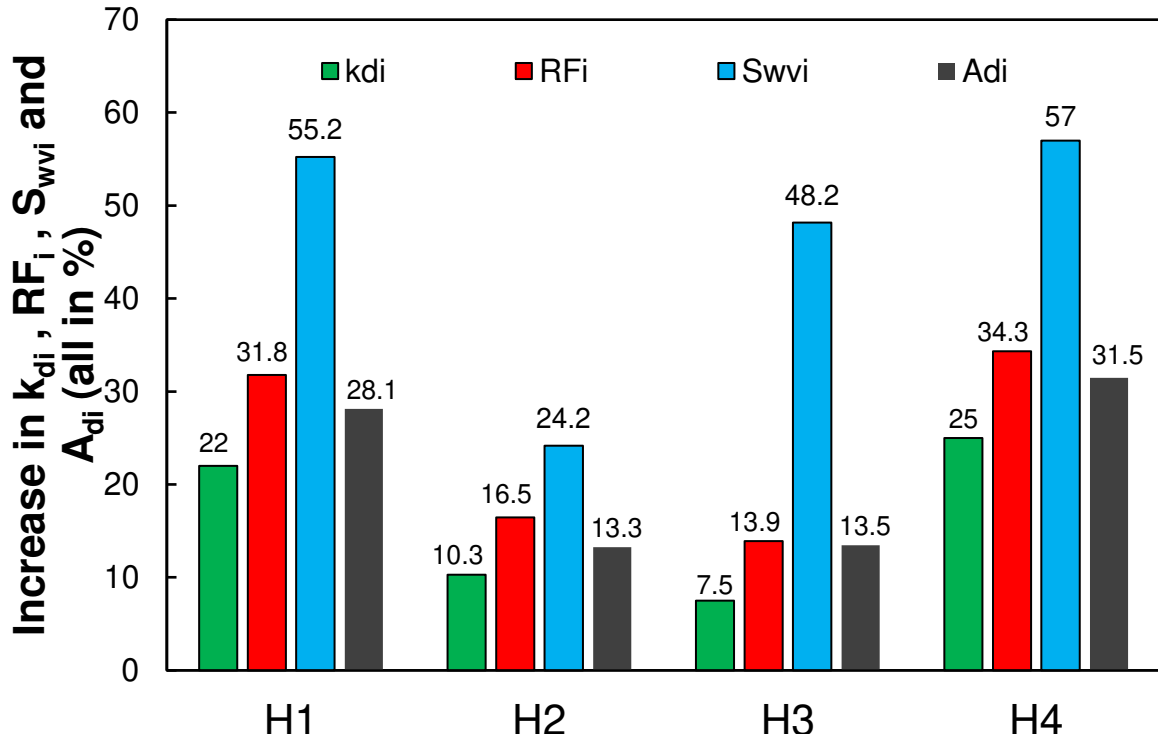


Figure 17. The increase in k_d , oil RF , S_{wv} and A_d for CO₂-SAG flooding presented in this paper compared with those for miscible CO₂ flooding^[13]. $k_{di} = (k_{d-CO_2-SAG} - k_{d-CO_2}) / k_{d-CO_2} \times 100\%$. $A_d, A_{di} = (A_{d-CO_2-SAG} - A_{d-CO_2}) / A_{d-CO_2} \times 100\%$. $S_{wv}, S_{wvi} = (S_{wv-CO_2-SAG} - S_{wv-CO_2}) / S_{wv-CO_2} \times 100\%$. $S_{wv}, RF_i = (RF_{CO_2-SAG} - RF_{CO_2}) / RF_{wv-CO_2} \times 100\%$.

Conclusions

- The process of the reservoir condition miscible CO₂-SAG process was studied for 4 cores with the same porosity but widely differing pore microstructure heterogeneities, and quantifying recovery factor, injection pressures, permeability damage and asphaltene precipitation. The data was compared to simple reservoir condition miscible CO₂ flooding on the same 4 cores and under the same conditions that we have already published.
- The oil recovery factors of CO₂-SAG flooding vary between 53 and 71%, depending on the heterogeneity of the cores. Overall recovery was 8-14% higher than miscible CO₂ flooding.
- The improvement in recovery associated with the use of CO₂-SAG flooding was strongest for rocks with heterogeneous pore microstructures whose miscible CO₂ performance was weakest. Consequently, it is proposed that CO₂-SAG injection is indicated for the improvement of the oil RFs of reservoirs with heterogeneous pore microstructures.
- It takes about 5 hours for the pressure to decay in the CO₂ soaking stage of the CO₂-SAG process. Rocks with homogeneous pore microstructures exhibited a greater initial pressure decay rate and a higher final pressure. It was found that the optimal time for ending the CO₂ soaking stage is about 80-135 minutes, which is linearly proportional to the fractal dimension which quantifies the heterogeneity of the pore microstructure.
- The permeability decline after CO₂-SAG flooding due to asphaltene precipitation is 8-19%, which is linearly proportional to the fractal dimension which quantifies the heterogeneity of the pore microstructure. The permeability decline after CO₂-SAG flooding is larger than that after CO₂ flooding (0.6–3.6%), while the corresponding permeability decline per unit percentage oil RF is smaller than that for CO₂ flooding.
- The changes in reservoir-critical macroscopic petrophysical properties, permeability decline and changes in wettability after CO₂-SAG are both significant. There is a permeability decline of 9-12% for CO₂-SAG flooding, higher than that for CO₂ flooding (6-9%). These changes are mainly due to larger wettability changes occurring with CO₂-SAG flooding, associated with the CO₂ soaking phase of the process. Cores with homogeneous pore microstructures experience a more pervasive penetration of CO₂, leading to larger changes in macroscopic petrophysical properties and consequently, to higher oil recoveries.

- The CO₂-SAG flooding process is a more reliable method for improving oil RFs which results in less damage to cores than miscible CO₂ flooding, and that is especially good for cores with poor pore-throat structure.

Acknowledgments

Thanks are given to the China Scholarship Council for funding the opportunity of the lead author to research at The University of Leeds, UK, and thanks to Professor Yang Shenglai from China University of Petroleum in Beijing for his guidance to the experiments. This research is supported By Open Fund (PLC2020007) of State Key Laboratory of Oil and Gas Reservoir Geology and Exploitation (Chengdu University of Technology).

References

- (1) Wang, R., Chi, Y., Zhang, L., He, R., Tang, Z. and Liu, Z., 2018. Comparative studies of microscopic pore-throat characteristics of unconventional super-low permeability sandstone reservoirs: Examples of Chang 6 and Chang 8 reservoirs of Yanchang Formation in Ordos Basin, China. *Journal of Petroleum Science and Engineering*, 160, pp. 72-90.
- (2) Liu, G., Meng, Z., Luo, D., Wang, J., Gu, D. and Yang, D., 2020. Experimental evaluation of interlayer interference during commingled production in a tight sandstone gas reservoir with multi-pressure systems. *Fuel*, 262, p.116557.
- (3) Lei, H., He, L., Li, R., Hu, Z. and He, J., 2019. Effects of boundary layer and stress sensitivity on the performance of low-velocity and one-phase flow in a shale oil reservoir: Experimental and numerical modeling approaches. *Journal of Petroleum Science and Engineering*, 180, pp.186-196.
- (4) Lai, J., & Wang, G., 2015. Fractal analysis of tight gas sandstones using high-pressure mercury intrusion techniques. *Journal of Natural Gas Science and Engineering*, 24, 185-196.
- (5) Al-Zainaldin, S., Glover, P.W.J. and Lorinczi, P., 2017. Synthetic Fractal Modelling of Heterogeneous and Anisotropic Reservoirs for Use in Simulation Studies: Implications on Their Hydrocarbon Recovery Prediction. *Transport in Porous Media*, 116(1), pp. 181-212.
- (6) Wang, H., Liu, Y., Song, Y., Zhao, Y., Zhao, J., & Wang, D., 2012. Fractal analysis and its impact factors on pore structure of artificial cores based on the images obtained using magnetic resonance imaging. *Journal of Applied Geophysics*, 86, 70-81.
- (7) Glover, P.W.J., Lorinczi, P., Al-Zainaldin, S., Al-Ramadhan, H., Daniel, G. and Sinan, S., 2018. Advanced fractal modelling of heterogeneous and anisotropic reservoirs, SPWLA 59th Annual Logging Symposium 2018.
- (8) Glover, P.W.J., Lorinczi, P., Al-Zainaldin, S., Al-Ramadhan, H., Sinan, S. and Daniel, G., 2019. A fractal approach to the modelling and simulation of heterogeneous and anisotropic reservoirs, Society of Petroleum Engineers - SPE Offshore Europe Conference and Exhibition 2019, OE.
- (9) Lei, H., Yang, S., Zu, L., Wang, Z. and Li, Y., 2016. Oil recovery performance and CO₂ storage potential of CO₂ water-alternating-gas injection after continuous CO₂ injection in a multilayer formation. *Energy & Fuels*, 30(11), pp.8922-8931.
- (10) Wang, Z., Yang, S., Lei, H., Yang, M., Li, L. and Yang, S., 2017. Oil recovery performance and permeability reduction mechanisms in miscible CO₂ water-alternative-gas (WAG) injection after continuous CO₂ injection: An experimental investigation and modeling approach. *Journal of Petroleum Science and Engineering*, 150, pp.376-385.
- (11) Qian, K., Yang, S., Dou, H., Wang, Q., Wang, L. and Huang, Y., 2018. Experimental investigation on microscopic residual oil distribution during CO₂ Huff-and-Puff process in tight oil reservoirs. *Energies*, 11(10), p. 2843.

- (12) Wang, Q., Yang, S., Lorinczi, P., Glover, P.W. and Lei, H., 2019. Experimental Investigation of Oil Recovery Performance and Permeability Damage in Multilayer Reservoirs after CO₂ and Water–Alternating–CO₂ (CO₂–WAG) Flooding at Miscible Pressures. *Energy & Fuels*, 34(1), 624–636.
- (13) Wang, Q., Yang, S., Glover, P.W., Lorinczi, P., Qian, K. and Wang, L., 2020. Effect of Pore–Throat Microstructures on Formation Damage during Miscible CO₂ Flooding of Tight Sandstone Reservoirs. *Energy & Fuels*, 34(4), 4338–4352.
- (14) Kord, S., Mohammadzadeh, O., Miri, R. and Soulgani, B.S., 2014. Further investigation into the mechanisms of asphaltene deposition and permeability impairment in porous media using a modified analytical model. *Fuel*, 117, pp. 259–268.
- (15) Lei, H., Yang, S., Qian, K., Chen, Y., Li, Y. and Ma, Q., 2015. Experimental investigation and application of the asphaltene precipitation envelope. *Energy & Fuels*, 29(11), pp. 6920–6927.
- (16) Qian, K., Yang, S., Dou, H.E., Pang, J. and Huang, Y., 2019. Formation damage due to asphaltene precipitation during CO₂ flooding processes with NMR technique. *Oil & Gas Science and Technology–Revue d'IFP Energies nouvelles*, 74, p.11.
- (17) Wang, L., He, Y., Chen, H., Meng, Z. and Wang, Z., 2019. Experimental investigation of the live oil–water relative permeability and displacement efficiency on Kingfisher waxy oil reservoir. *Journal of Petroleum Science and Engineering*, 178, pp.1029–1043.
- (18) Christensen, J.R., Stenby, E.H. and Skauge, A., 1998. Review of WAG field experience. In *International Petroleum Conference and Exhibition of Mexico*. Society of Petroleum Engineers.
- (19) Grogan, A.T. and Pinczewski, W.V., 1987. The role of molecular diffusion processes in tertiary CO₂ flooding. *Journal of petroleum technology*, 39(05), pp.591–602.
- (20) Sohrabi, M., Riazi, M., Jamiolahmady, M., Kechut, N.I., Ireland, S. and Robertson, G., 2011. Carbonated water injection (CWI)—A productive way of using CO₂ for oil recovery and CO₂ storage. *Energy Procedia*, 4, pp.2192–2199.
- (21) Ma, Q., Yang, S., Lv, D., Wang, M., Chen, J., Kou, G. and Yang, L., 2019. Experimental investigation on the influence factors and oil production distribution in different pore sizes during CO₂ huff–n–puff in an ultra–high–pressure tight oil reservoir. *Journal of Petroleum Science and Engineering*, 178, pp.1155–1163.
- (22) Wang, Q., Lorinczi, P. and Glover, P.W., 2020. Oil production and reservoir damage during miscible CO₂ injection. *The Leading Edge*, 39(1), pp.22–28.
- (23) Zhang, J., Zhang, H.X., Ma, L.Y., Liu, Y. and Zhang, L., 2020. Performance evaluation and mechanism with different CO₂ flooding modes in tight oil reservoir with fractures. *Journal of Petroleum Science and Engineering*, p.106950.
- (24) Li, Z. and Gu, Y., 2014. Soaking effect on miscible CO₂ flooding in a tight sandstone formation. *Fuel*, 134, pp. 659–668.
- (25) Li, Z., 2014. Optimum Timing for CO₂–EOR After Waterflooding and Soaking Effect on Miscible CO₂ Flooding in a Tight Sandstone Formation (Doctoral dissertation, Faculty of Graduate Studies and Research, University of Regina).
- (26) Wang, L., He, Y., Peng, X., Deng, H., Liu, Y. and Xu, W., 2020. Pore structure characteristics of an ultradeep carbonate gas reservoir and their effects on gas storage and percolation capacities in the Deng IV member, Gaoshiti–Moxi Area, Sichuan Basin, SW China. *Marine and Petroleum Geology*, 111, pp. 44–65.
- (27) Luo, M., Glover, P.W. and Pan, H., 2019. A reassessment of the stress and natural fracture orientations from analysis of image logs in the Chinese Continental Scientific Drilling Program borehole at Donghai county, Jiangsu province, China. *Journal of Asian Earth Sciences*, 169, pp.11–20.
- (28) Glover, P.W.J. and Walker, E., 2008. Grain–size to effective pore–size transformation derived from electrokinetic theory. *Geophysics*, 74(1), pp. E17–E29.
- (29) Cao, M. and Gu, Y., 2013. Oil recovery mechanisms and asphaltene precipitation phenomenon in immiscible and miscible CO₂ flooding processes. *Fuel*, 109, pp.157–166.
- (30) Li, Z. and Dong, M., 2009. Experimental study of carbon dioxide diffusion in oil–saturated porous media under reservoir conditions. *Industrial & engineering chemistry research*, 48(20), pp.9307–9317.
- (31) Yang, D., Gu, Y. and Tontiwachwuthikul, P., 2008. Wettability determination of the reservoir brine–reservoir rock system with dissolution of CO₂ at high pressures and elevated temperatures. *Energy & Fuels*, 22(1), pp.504–509.

- (32) Wang, Q., Yang, S., Han, H., Wang, L., Qian, K. and Pang, J., 2019. Experimental Investigation on the Effects of CO₂ Displacement Methods on Petrophysical Property Changes of Extra-Low Permeability Sandstone Reservoirs near Injection Wells. *Energies*, 12(2), p. 327.
- (33) Lai, J., & Wang, G., 2015. Fractal analysis of tight gas sandstones using high-pressure mercury intrusion techniques. *Journal of Natural Gas Science and Engineering*, 24, 185-196.
- (34) Wu, H., Zhang, C., Ji, Y., Liu, R., Wu, H., Zhang, Y., Geng, Z., Zhang, Y. and Yang, J., 2018. An improved method of characterizing the pore structure in tight oil reservoirs: Integrated NMR and constant-rate-controlled porosimetry data. *Journal of Petroleum Science and Engineering*, 166, pp. 778-796.
- (35) Cao, M. and Gu, Y., 2013. Physicochemical characterization of produced oils and gases in immiscible and miscible CO₂ flooding processes. *Energy & Fuels*, 27(1), pp. 440-453.
- (36) Sim, S.S.K., Okatsu, K., Takabayashi, K. and Fisher, D.B., 2005, January. Asphaltene-induced formation damage: effect of asphaltene particle size and core permeability. In *SPE Annual Technical Conference and Exhibition. Society of Petroleum Engineers*.
- (37) Iglauer, S., Fernø, M.A., Shearing, P. and Blunt, M.J., 2012. Comparison of residual oil cluster size distribution, morphology and saturation in oil-wet and water-wet sandstone. *Journal of colloid and interface science*, 375(1), pp.187-192.
- (38) Uetani, T., 2014. Wettability alteration by asphaltene deposition: A field example. In *Abu Dhabi International Petroleum Exhibition and Conference. Society of Petroleum Engineers*.
- (39) Okwen, R.T., 2006, January. Formation Damage by CO₂ Asphaltene Precipitation. In *SPE International Symposium and Exhibition on Formation damage control. Society of Petroleum Engineers*.